Space-Time Spectral Analysis of Mid-Latitude Disturbances Appearing in a GFDL General Circulation Model

Y. HAYASHI AND D. G. GOLDER

Geophysical Fluid Dynamics Laboratory, NOAA, Princeton University, Princeton, N. J. 08540

(Manuscript received 22 June 1976, in revised form 8 October 1976)

ABSTRACT

A space-time spectral analysis is applied to the Northern Hemisphere winter of an 11-layer GFDL general circulation model with seasonal variation. A statistical study is made of the stationary and transient ultra-long waves and transient long waves with respect to their wave characteristics, three-dimensional structure and energetics.

The stratospheric stationary waves attain their maximum amplitude in geopotential at the latitudes of the stratospheric jet in agreement with observations and theories, although their amplitude is too large. The tropospheric stationary waves corresponding to the Siberian high and the Aleutian low are characterized by large eddy available potential energy which is mainly converted from zonal available potential energy. On the other hand, the tropospheric stationary wave corresponding to the local intensification of the subtropical jet is characterized by large eddy kinetic energy which is supplied by the energy flux from the region of large eddy energy conversion occurring to the north of the latitude of the Tibetan Plateau.

The transient ultra-long waves are too weak in the troposphere and are associated with a more eastward moving component contrary to those observed in the troposphere. They are characterized by baroclinic energy conversion in the troposphere and barotropic conversion in the stratosphere.

The transient long waves corresponding to cyclones are well simulated and their phase relations agree with both observations and linear theories. Their kinetic energy is largest around 300 mb in agreement with observations, but contrary to linear theories. Their kinetic energy maxima occur over the Pacific and the Atlantic to the east of the maximum latitudinal gradient of the time mean temperature.

1. Introduction

In recent years, remarkable progress has been made in the development of general circulation models. These models together with observational and theoretical studies have made invaluable contributions to the simulation and understanding of larg-scale atmospheric phenomena. They yield an abundance of output data both in space and time and also provide vertical velocity and heating which are not directly observable. This study is a comprehensive space-time spectral analysis of mid-latitude disturbances appearing in the Northern Hemisphere winter of a GFDL global general circulation model (Manabe *et al.*, 1974), extending the previous spectral analysis of tropical disturbances (Hayashi, 1974). For the gross statistics of mid-latitude disturbances in a general circulation model with and without mountains, the reader is referred to Manabe and Terpstra (1974) which provides a framework for the present analysis.

Large-scale mid-latitude waves may be classified into stationary and transient ultra-long waves (wavenumbers 1–3) and long waves (wavenumbers 5–7). The stationary ultra-long waves have been theoretically interpreted as waves forced thermally and/or orographically [see a review by Saltzman (1968)]. Charney and Eliassen (1949), Bolin (1950) and Gambo (1956) demonstrated by barotropic models that stationary waves are produced by flow over mountains. On the other hand, Smagorinsky (1953), Döös (1962) and Murakami (1967) concluded that thermal effects account for the essential features of the observed distribution of sea level pressure, while the relative importance of mountain effects increases with increasing altitude. The effects of mountains and heating were also studied theoretically by Sankar-Rao (1965), Sankar-Rao and Saltzman (1969), Derome and Wiin-Nielsen (1971) and Egger (1976a,b).

Recently, general circulation models have also produced interesting results concerning the generation of stationary waves. The mountains in these models have not only a lifting effect but also a blocking effect on the air. Mintz (1965) suggested that the Tibetan Plateau is responsible for maintaining the Siberian high during the winter, based on the Mintz-Arakawa general circulation model with realistic orography. Kasahara and Washington (1971), based on a NCAR general circulation model, concluded that thermal rather than orographic effects are the dominating factor which determines the stationary flow in the troposphere, while orographic effects become important in the

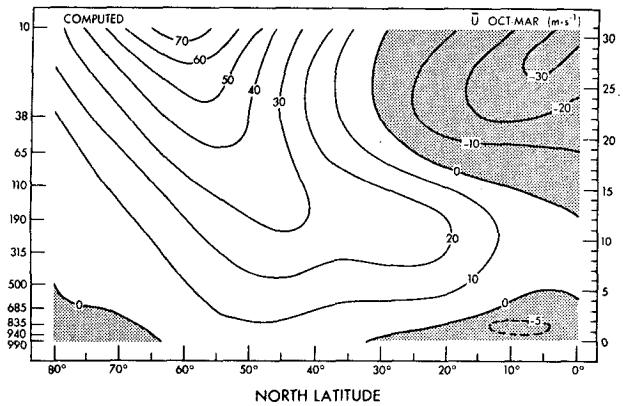

FIG. 3.1a. Latitude-height section [pressure (mb) left, height (km) right] of the mean zonal wind of the model atmosphere during the period October–March.

stratosphere (Kasahara *et al.*, 1973; J. Williams, 1976). On the other hand, Manabe and Terpstra (1974) concluded, based on a GFDL general circulation model, that stationary waves are substantially enhanced by the effect of mountains not only in the stratosphere but also in the troposphere through an increase in energy conversion from available potential energy. They also found that the location of the Siberian high shifts southward if the Tibetan Plateau is taken out. In the present study, it will be of interest to make a detailed analysis of the three-dimensional structure and energetics of stationary waves in a general circulation model which incorporates internally determined diabatic heating and realistic orography. It is also a point of interest to examine how the energy of the simulated stationary waves propagates through the horizontal and vertical wind shear as has been studied theoretically by Eliassen and Palm (1960), Charney and Drazin (1961), Dickinson (1968), Matsuno (1970), Clark (1972), Simmons (1974a) and Garcia and Geisler (1974) [see also a review by Holton (1975)].

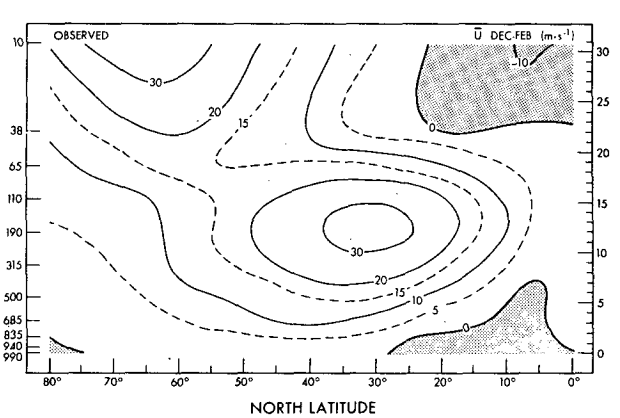

FIG. 3.1b. Latitude-height section of the mean zonal wind of the real atmosphere during the period December–February (after Newell *et al.*, 1970).

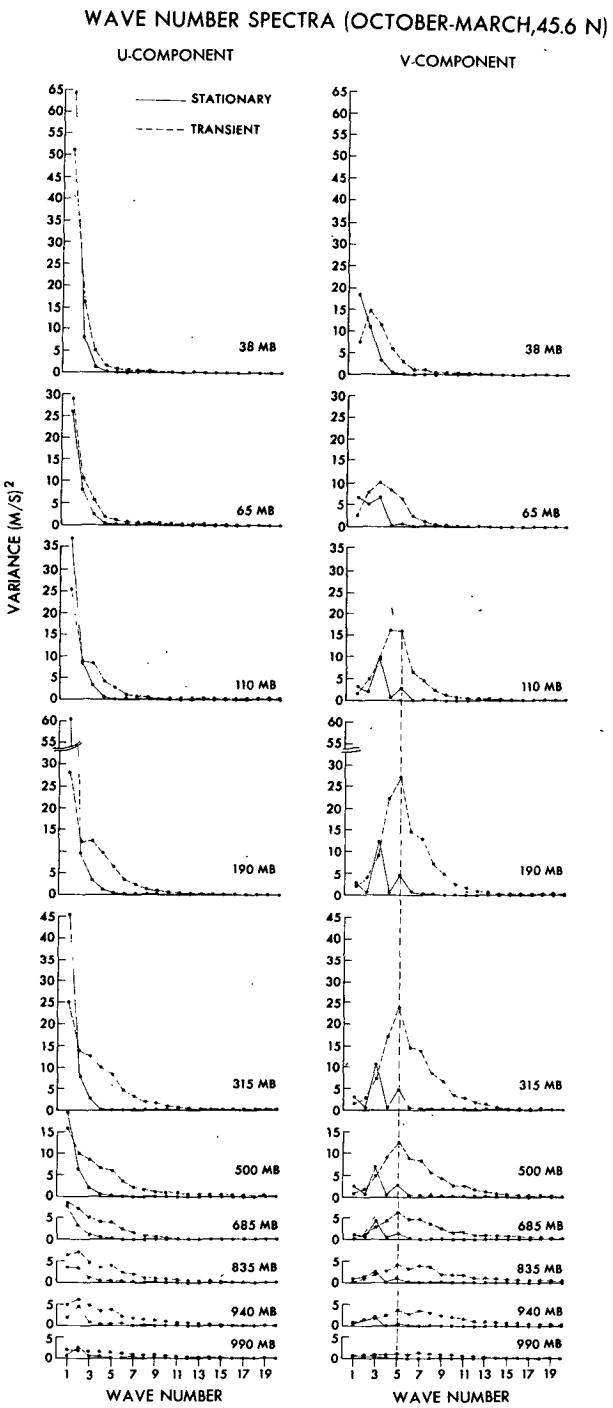

FIG. 4.1. Model wavenumber power spectra of zonal component (left) and meridional component (right) of the wind at 45.6°N. Full and dashed lines show variance spectra for stationary and transient waves, respectively.

Transient ultra-long waves may play an important role in long-range weather forecasting. These waves have been studied for the real atmosphere by Kubota and Iida (1954), Deland (1964, 1965a,b, 1972, 1973a,b), Deland and Liu (1967), Deland and Johnson (1968),

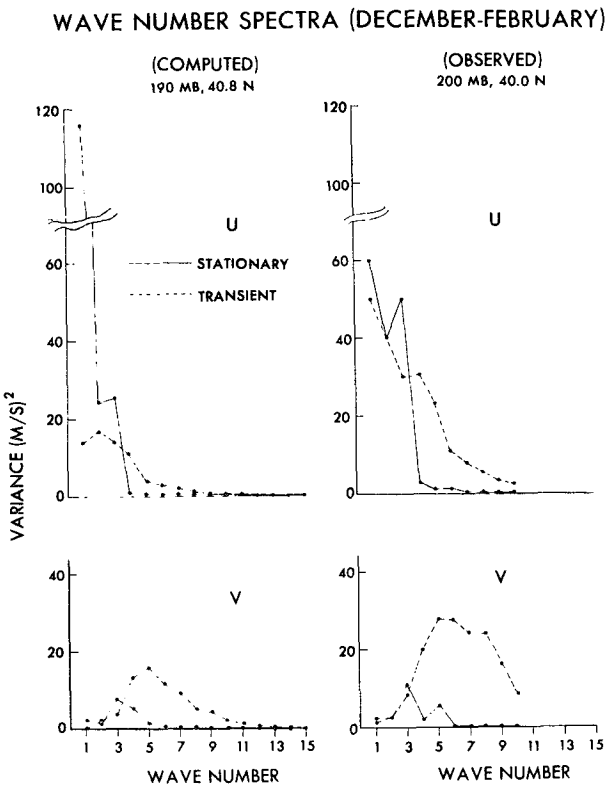

Fig. 4.2. Model (left) and observed (right) wavenumber power spectra of zonal (top) and meridional (bottom) wind during the period December–February 1964. The observed power spectra are adapted from Kao and Wendell (1970) with the values doubled as corrected by Willson (1975).

Eliasen and Machenhauer (1965, 1969), Arai (1965, 1971, 1973), Bradley and Wiin-Neilsen (1968), Kao and Wendell (1970), Kao *et al.* (1970), Iwashima (1973, 1974) and Pratt and Wallace (1976). However, the three-dimensional structure of these waves is not well explored. There are only a few theoretical studies relevant to these waves. According to Green (1960), Burger (1962), Hirota (1968b), Garcia and Norscini (1970) and Geisler and Dickinson (1975), baroclinic instability also occurs at very long wavelengths and higher vertical modes. Numerical experiments by Brown (1969a,b), Song (1971a,b), Simons (1972) and Gall (1976a) have shown that barotropic instability is possible at very long wavelengths in the presence of both horizontal and vertical shear. However, such unstable ultra-long waves are associated with small growth rates and move eastward in the westerlies while observed ultra-long waves have significant amplitude and generally move westward (Kubota and Iida, 1954). Hirota (1971) suggested that traveling ultra-long waves in the stratosphere are excited by a periodic fluctuation of tropospheric stationary waves forced by a pulsating zonal flow over mountains. On the other hand, Manabe and Terpstra (1974) demonstrated by their general curculation model that although stationary waves are enhanced by the effect of mountains, transient ultra-long waves are reduced in the troposphere. In the present study it will be of interest to examine whether the transient ultra-long waves appearing in a general circulation model correspond to those studied observationally or theoretically.

Transient long waves may essentially be explained by baroclinic instability (Bjerknes and Holmboe, 1944; Charney, 1947; Eady, 1949; Fjortoft, 1951; Kuo, 1952, 1953, 1973; G. P. Williams, 1974) in the presence of vertical shear rather than barotropic instability (Kuo, 1949) in the presence of horizontal wind shear. The combined barotropic-baroclinic instability in the presence of both horizontal and vertical shear (Charney and Stern, 1962; Pedlosky, 1964a,b; Stone, 1969; Brown, 1969a,b; McIntyre, 1970; Song, 1971a,b) predicts that the long waves gain energy from potential energy by the baroclinic process, while they lose energy to the zonal flow by the barotropic process.

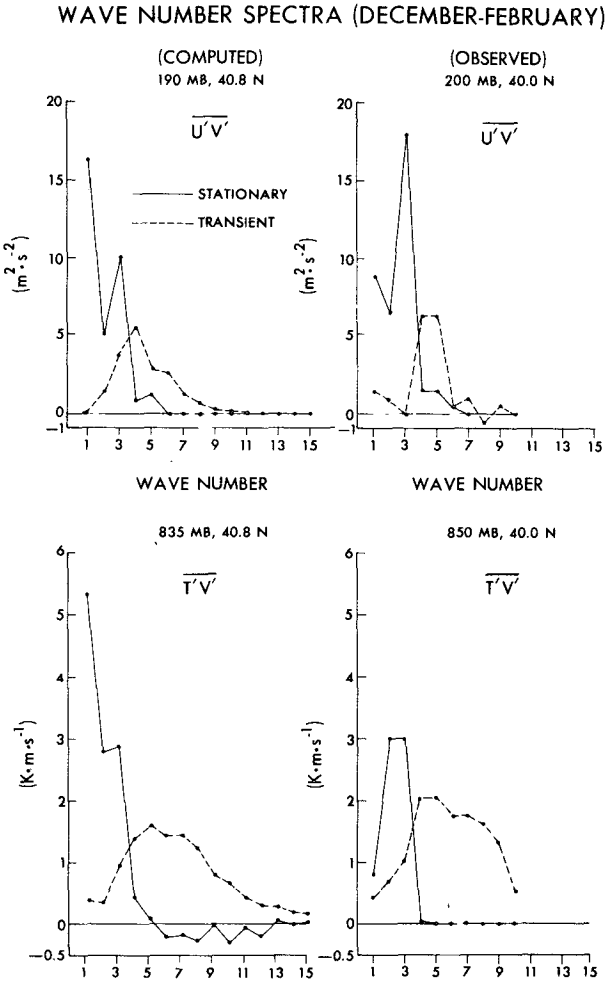

FIG. 4.3. Model (left) and observed (right) co-spectra of meridional flux of momentum (top) and sensible heat (bottom) during the period December–February 1964. The observed momentum and heat fluxes are adapted from Kao *et al.* (1970) and Kao and Sagendorf (1970), respectively.

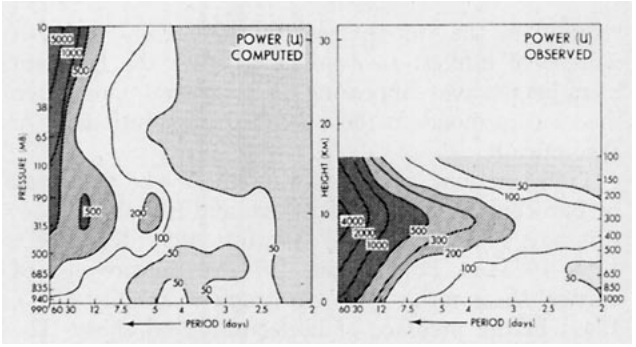

FIG. 4.4a. Frequency-height section of power spectra of the zonal component: left, computed at 52.8°N, 33°W; right, observed at 53.0°N, 35°W, a 13-winter average (adapted from Hartmann, 1974).

Recently, Simons (1972), Gall (1976a) and Simmons and Hoskins (1976) studied the combined barotropic-baroclinic instability based on a more realistic zonal flow and static stability. In particular, Gall (1976a), based on a linear experiment with a GFDL general circulation model, found that the initial growth rate attains its maximum at wavenumbers 12–15 rather than at wavenumbers 5–7, which had been predicted by previous linear theories. Moreover, the long waves (wavenumbers 5–7) attain their maximum geopotential amplitude near the surface with a secondary maximum in the upper troposphere, whereas the observed maximum occurs in the upper troposphere. Gall (1976b,c) further demonstrated that linear theories can explain only the initial growth and structure for the first 3–4 days, while the preferred scale and structure at the mature stage can be simulated by the nonlinear equations. In the present study it will be of interest to examine the three-dimensional structure of long waves appearing in a general circulation model which is based on a set of nonlinear equations with zonally varying vertical and horizontal wind shear.

2. Brief description of the model

The global model chosen for this study was constructed by Manabe and Holloway primarily to investigate the seasonal variation of climate (Manabe *et al.*, 1974; Manabe and Mahlman, 1976). It has 11 levels and an interval of 2.4° between the horizontal grids developed by Kurihara and Holloway (1967) and modified by Holloway and Manabe (1971). The seasonal variation of solar radiation and sea surface temperature is prescribed. The temperature at the land surfaces is determined in such a way that it satisfies a condition of heat balance. The effect of moist convection is represented by moist convective adjustment (Manabe *et al.*, 1965). Mountains are incorporated by the use of the sigma coordinate system (Phillips, 1957).

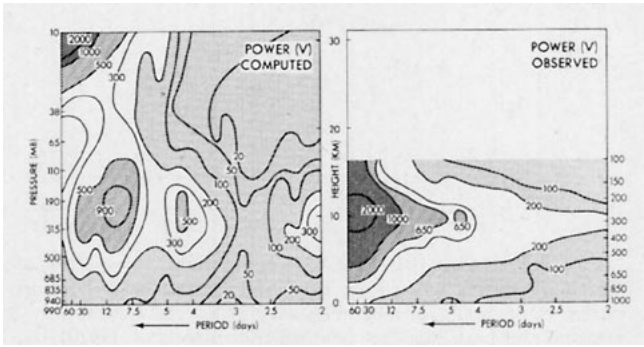

FIG. 4.4b. As in Fig. 4.4a except for the meridional component.

3. Mean zonal wind

Since waves are sensitive to the zonal mean state, the model's mean zonal wind (Fig. 3.1a) is compared to that observed (Fig. 3.1b) by Newell *et al.* (1970). In the model, the jet stream in the northern stratosphere is too strong by a factor of more than 2, while the subtropical jet around 30°N is not pronounced.

4. Classification of mid-latitude waves

a. Wavenumber analysis

In order to determine the characteristic scale of the model's mid-latitude stationary and transient waves, a wavenumber analysis was performed during the period from October through March. "Stationary" is defined as a 6-month mean, while "transient" is defined as a deviation from this mean. For wavenumber analyses of observed mid-latitude waves, see reviews by Van Mieghem (1961) and Saltzman (1970).

Fig. 4.1 shows the wavenumber spectra of stationary and transient waves for various levels at 45.6°N. Stationary ultra-long waves are associated with a major spectral peak at wavenumber 1 in the zonal component of the wind above 835 mb and a minor peak at wavenumber 3 in the meridional component below 65 mb. This minor peak does not appear in a model without mountains (see Manabe and Terpstra, 1974). On the other hand, transient waves are associated with a peak at wavenumber 1 in the zonal component above 835 mb corresponding to transient ultra-long waves and also a significant spectral peak at wavenumber 5 below 65 mb in the meridional component corresponding to transient long waves. The peak at wavenumber 5 of transient waves is seen only up to 110 mb, consistent with the wave propagation theory (Charney and Drazin, 1961; Charney and Pedlosky, 1963; Holton, 1973) that long waves cannot penetrate into regions of strong westerlies.

In Fig. 4.2, wavenumber spectra at 190 mb are compared with those observed (Kao and Wendell, 1970), confirming that the spectral peaks in the model occur at the observed characteristic wavenumbers. However, the model's stationary ultra-long waves are too strong, its transient ultra-long waves too weak, and the transient long waves somewhat weaker compared to those

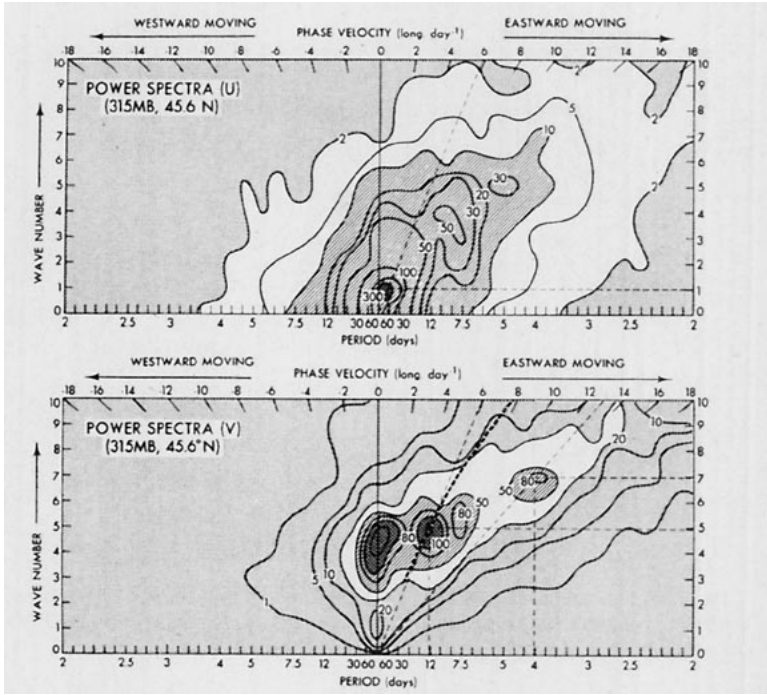

FIG. 4.5. Frequency-wavenumber section of power spectrum density (m^2 s^{-2} day^{-1}) of zonal component (upper) and meridional component (lower) at 315 mb, 45.6°N. The thick dashed line in the lower diagram indicates the wavenumber-frequency expected from a linear instability theory (after Gall, 1976a).

observed. This conclusion is not altered, even if the observed wave activity varies from year to year (not illustrated).

In Fig. 4.3, wavenumber cospectra of the horizontal flux of momentum and sensible heat are compared to those observed by Kao *et al.*, (1970) and Kao and Sagendorf (1970), respectively. It is seen that both momentum and sensible heat flux of the model's stationary waves are associated with a primary peak at wavenumber 1 and a secondary peak at wavenumber 3, whereas the observed fluxes of momentum and sensible heat are characterized by a primary peak at wavenumber 3. On the other hand, both the model's and the observed transient momentum and sensible heat fluxes are characterized by a spectral peak at wavenumbers 4–5.

b. Frequency analysis

In order to examine the characteristic time scale of the transient waves a conventional time-power spectral analysis of the model's data has been made. Figs. 4.4a, and 4.4b show a time-power spectrum density (variance per unit frequency) of the model's zonal and meridional wind components, respectively, compared to those observed (Hartmann, 1974). This comparison confirms that the model's transient ultra-long waves associated with periods of 30–60 days are too weak compared to those observed. Since these long-period oscillations are weak, spectral peaks at 4–5 day and 12 day periods are clearly seen in the model. The 12-day period may be interpreted as a time interval between rather strong cyclones, while the 4–5 day period is due to weaker cyclones. However, the observed data show a rather vague spectral peak at 4–5 day periods and no isolated peak at 12-day periods. In the paper of Hartmann (1974), the long-period oscillations look weaker and the 4–5 day peak appears sharper than those in Fig. 4.4, since he employed a logarithmic representation of power spectrum which is multiplied by frequency. In both representations the power spectrum drops sharply for periods <4 days.

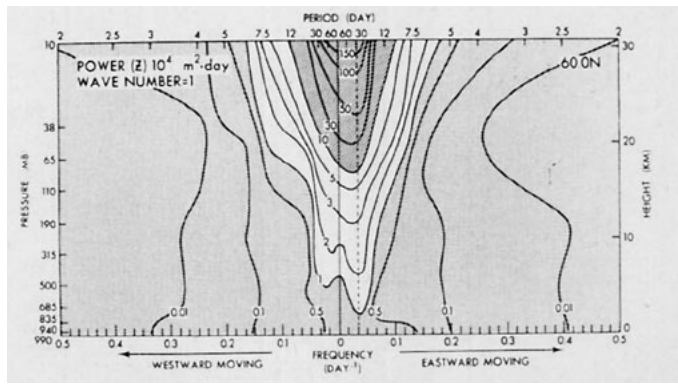

FIG. 4.6. Frequency-height section of the power spectrum density of geopotential height (wavenumber 1) at 60°N.

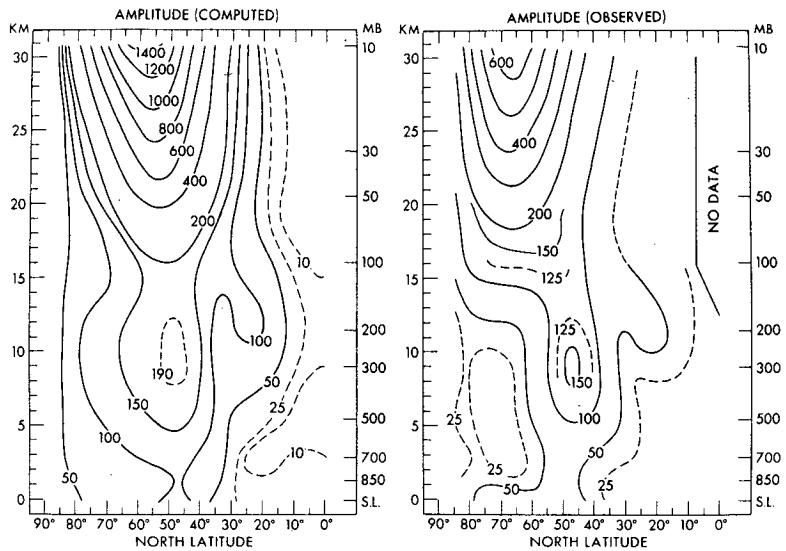

FIG. 5.1a. Latitude-height section of the amplitude (m) of stationary geopotential height (wavenumber 1) in January: left, model wave; right, observed wave (monthly average of several years) after van Loon *et al.* (1973).

c. *Wavenumber-frequency analysis*

When dealing with linear theories, disturbances are assumed to take the form of sinusoidal waves in longitude and time. Their phase speeds, preferred scale and structure of the wave solution are then examined. In the case of a nonlinear experiment with a nonuniform basic state, disturbances are no longer simple sinusoidal waves. However, it is still of interest to analyze these disturbances in their wavenumber-frequency domain and compare them with the results of linear theories and those observed. For this purpose, we shall make use of the space-time cross spectral analysis technique developed by Hayashi (1971, 1973, 1977). Wavenumber-frequency analysis of observed mid-latitude disturbances was first performed by Kao and Wendell (1970), based on the two-dimensional direct Fourier transform method presented by Kao (1968). The present method gives additional information of phase and coherence. A lag correlation method with a 30-day lag was used in the present computation.

The power spectra of the wind components in the wavenumber-frequency domain are given in Fig. 4.5. The upper diagram reveals that transient ultra-long waves of the zonal component of the wind at 315 mb, 45.6°N are associated with wavenumber 1, moving eastward with a period of about 60 days. The meridional

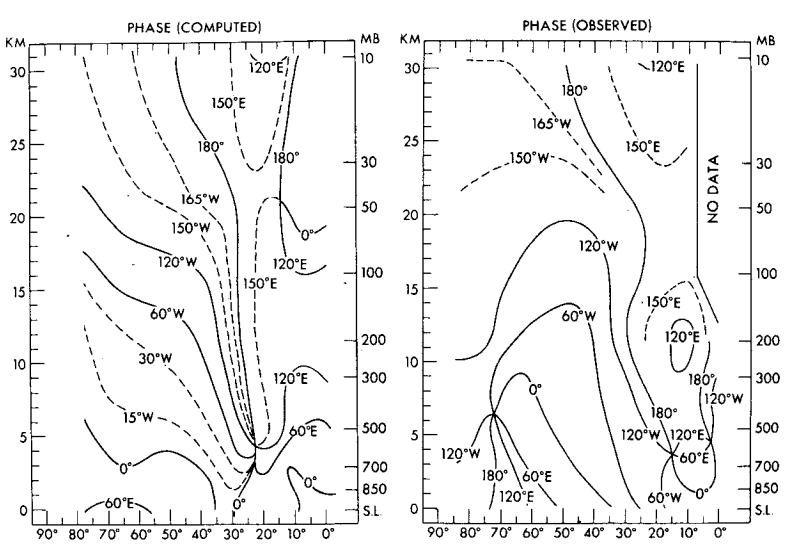

FIG. 5.1b. As in Fig. 5.1a except for the phase (longitude of ridge).

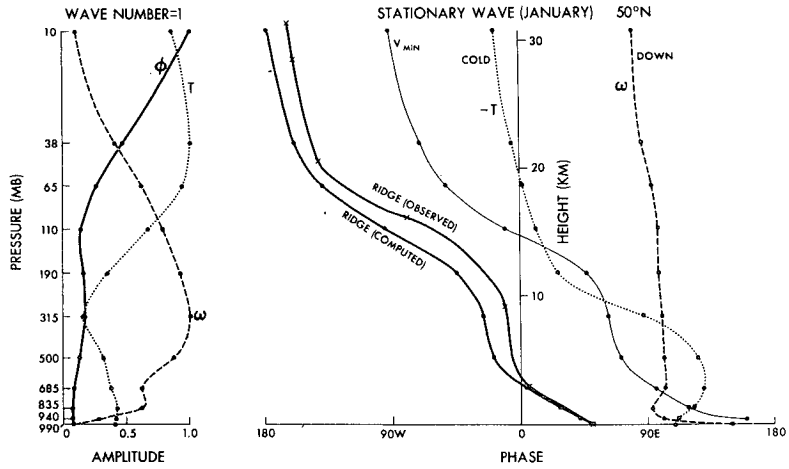

FIG. 5.2. Vertical profile of normalized amplitude (left) and phase (right) of the stationary wave (wavenumber 1) at 50°N. Observed phase line (ridge) is taken from Muench (1965) for January 1958 at 50°N.

component, shown in the lower diagram, indicates that transient long waves take the form of a wave packet consisting of a broad spectrum of wavenumbers and frequencies with an eastward phase velocity. Two representative spectral peaks are seen, one at wavenumber 5 with a period of 12 days corresponding to strong cyclones, the other at wavenumber 7 and period of 4 days corresponding to weak cyclones. We would now like to see if these wavenumber-frequency relations agree with linear theory.

Recently, Gall (1976a) conducted a linear experiment with a general circulation model, using for the basic state, winds and temperatures given by the present model. The resulting dispersion curve of this model's stable waves is entered in the lower diagram of Fig. 4.5. As indicated in this diagram, the peak at wavenumber 5 (12 day period) falls on this curve. However, the peak at wavenumber 7 does not, and is associated with shorter periods than predicted by his linear experiment.

The power spectrum of the geopotential height of wavenumber 1 at 60°N is shown in Fig. 4.6 as a function of frequency and height. According to this figure, the ultra-long waves are associated with more eastward than westward moving components at all levels. This is contrary to observed ultra-long waves in the troposphere which are associated with more westward moving components (see Deland, 1964). In the stratosphere, however, recent observational analysis by Sato (1976) reveals a more eastward moving component for wavenumber 1 in the years 1966 and 1967.

In the following sections a detailed analysis will be made of the model's stationary and transient ultra-long waves and transient long waves with respect to their three-dimensional structure and energetics.

5. Analysis of stationary ultra-long waves

a. Three-dimensional structure

The meridional sections shown in Fig. 5.1 compare the distributions of amplitude and phase of the stationary wave (for geopotential height, wavenumber=1) of the model to those observed (van Loon *et al.*, 1973).

The location of the tropospheric maxima of amplitude occur at 200–300 mb around 50°N and 25°N, in good agreement with those observed except that the model's amplitude is somewhat larger. On the other hand, the model's stratospheric maximum occurs about 10° south of that observed and its amplitude is too large by a factor of more than 2. This stratospheric maximum of the geopotential amplitude coincides with the maximum westerlies as presented in Fig. 3.1a. In this respect, the model agrees with both observations (Hirota and Sato, 1969; van Loon *et al.*, 1973) and theories (Matsuno, 1970; Simmons, 1974) using realistic basic winds. However, it does not agree with the theory using idealistic basic winds by Dickinson (1968) in which the geopotential maximum occurs to the north of the westerly maximum as pointed out by Simmons (1974a).

Fig. 5.1b indicates that the model's geopotential phase lines tilt westward with height in middle latitudes in agreement with those observed. The horizontal phase line tilts from southwest to northeast between 30°N and 80°N, whereas, observationally, a reversal in the horizontal tilt occurs around 50°N. One can also note that around 30°N there is a rapid variation in the horizontal phase both in the model and observed atmospheres.

The vertical structure of the stationary wave is illustrated in Fig. 5.2. The ridge lines can be seen to tilt westward with height in good agreement with observed data by Muench (1965) which is entered in

the same figure. This westward tilt with height implies, according to the relation by Eliassen and Palm (1960), that energy is transported from the troposphere to the stratosphere in agreement with observations (Reed *et al.*, 1963; Oort, 1964). Fig. 5.2 also shows that the stratospheric stationary wave is 180° out of phase with the tropospheric stationary wave except for their vertical velocities. This phase shift occurs around 110 mb where the geopotential amplitude becomes small. This node can be interpreted as a result of the reflection of the stationary wave by the strong stratospheric westerlies as discussed observationally by Sato (1974).

The ridge is situated about 90° to the west of the downward motion (divergence) in the troposphere, while it is situated about 90° to the west of the upward motion (divergence) in the stratosphere. This feature is consistent with the quasi-geostrophic vorticity equation in the absence of friction,

$$\left(\frac{\partial}{\partial t}+\bar{U}\frac{\partial}{\partial x}\right)\nabla^2\phi+\beta\frac{\partial\phi}{\partial x}=f^2\frac{\partial\omega}{\partial p}, \tag{5.1}$$

which implies that the ridge occurs 90° to the *east* or *west* of the divergence $(-\partial\omega/\partial p)$ associated with stationary or traveling waves. Furthermore, for ultra-long waves, the time derivative and advective terms may be neglected according to the scale analysis by Burger (1958) as

$$\beta\frac{\partial\phi}{\partial x}=f^2\frac{\partial\omega}{\partial p}; \tag{5.2}$$

which indicates that the ridge occurs 90° to the *west* of divergence $(-\partial\omega/\partial p>0)$.

Here, it is also of interest to point out the phase relations near the Tibetan Plateau with respect to energetics. Fig. 5.2 indicates that around 90°E in the troposphere a northerly wind is associated with cold air. Therefore, the meridional flux of sensible heat is poleward $(\overline{T'v'}>0)$ which in turn suggests that there is a conversion of energy from zonal available potential energy to eddy available potential energy $[-(\partial\bar{T}/\partial y)\overline{T'v'}>0]$. Further examination of Fig. 5.2 reveals that sinking motion is associated with cold air $(-\overline{T'\omega'}>0)$ indicating that the eddy available potential energy is further converted into eddy kinetic energy. This point will be discussed quantitatively in the next section on energetics.

In order to visualize the three-dimensional structure of the stationary waves, a synoptic analysis is presented in Fig. 5.3. The time-mean height contours in Fig. 5.3a are composed of wavenumbers 1, 2, 3. One can see that the high and low occur around 50–60°N at levels 38, 190 and 940 mb, consistent with the results of the spectral analysis (Fig. 5.1a). On the other hand, Fig. 5.3b depicts how these stationary ultra-long waves appear in a time-mean synoptic map with the zonal mean included. Interestingly, the high is shifted southward, while the low is shifted northward due to the latitudinal gradient of the zonal mean geopotential height.

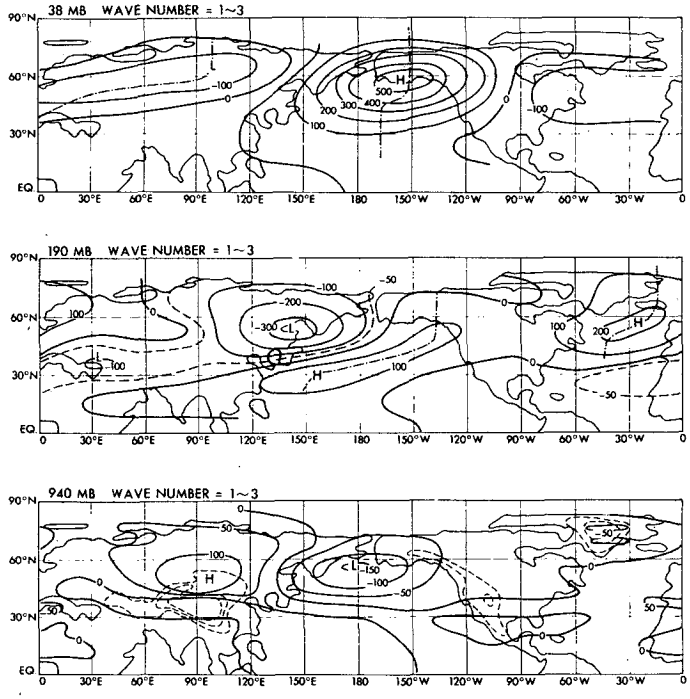

FIG. 5.3a. Map of time-mean heights (m) composed of wavenumbers 1–3 (top) during the period October–March at 38, 190 and 940 mb. The dashed lines in the bottom figure indicate topography.

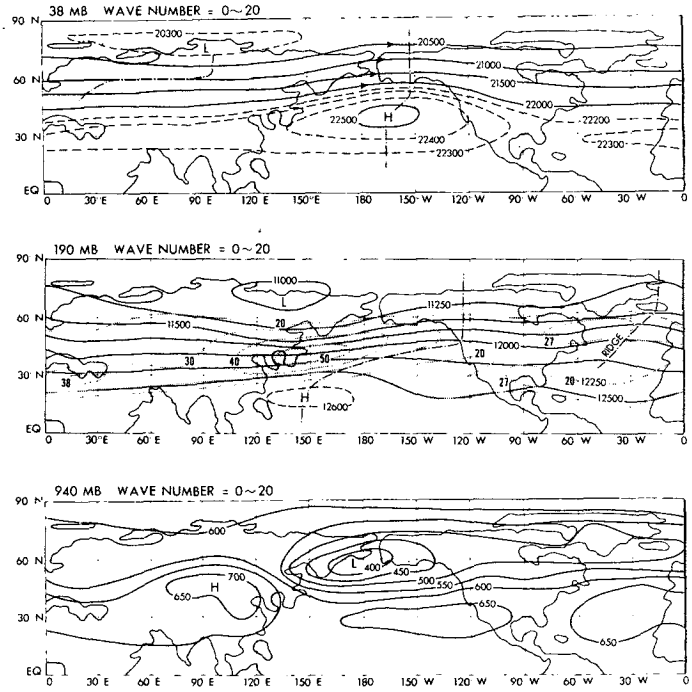

FIG. 5.3b. As in Fig. 5.3a except for wavenumbers 0–20. The dotted lines in the middle figure show the zonal wind (m s^{-1}).

In Fig. 5.3a, one can see that the high and low at 38 mb appear to the west of their counterparts at 190 mb, consistent with the westward tilt of the geopotential phase line with height. At 190 mb in Fig. 5.3a, an additional high appears over the Pacific, situated east of the Tibetan Plateau, with a horizontal axis running southwest to northeast. This corresponds to the minor maximum of the geopotential amplitude of wavenumber 1 at 190 mb (Fig. 5.1a) and the rapid variation in the horizontal phase (Fig. 5.1b). If the zonal mean is included (Fig. 5.3b) the geopotential height gradient at 190 mb looks very strong between the low and high around 150°E and the zonal velocity (dotted isopleths) becomes extremely large, corresponding to the strengthening of the westerly jet stream to the east of the Tibetan Plateau. This large zonal velocity accounts for the large power spectra of the zonal component which will be shown in Fig. 5.5b.

At 940 mb in Fig. 5.3a, one can see the anticyclone known as the Siberian high is formed north of the Tibetan Plateau and the Aleutian low is formed over the Bering Sea.

It is also of interest here to examine the distribution of the vertical velocity of the stationary wave in the lower troposphere and see whether it is appreciably affected by the flow over mountains or frictional convergence within the Ekman layer. The upper diagram of Fig. 5.4, illustrating the model's time-mean isopleths of the vertical p-velocity for wavenumbers 0–20, shows that strong sinking motion occurs northeast of the Tibetan Plateau near Manchuria, while rising motion occurs in the northeast Pacific. The lower diagram is adapted from Saltzman and Irsch (1972) who computed the topographically induced vertical velocity at the surface based on the observed horizontal wind [see also Fig. 7 in Egger (1976a)]. According to this figure, a maximum sinking motion occurs to the lee side of the Tibetan Plateau. This comparison suggests that the model's vertical velocity of the stationary wave at 940 mb is not appreciably affected by the flow over the mountains. Instead, this sinking motion is associated with the horizontal divergence of flows around the Tibetan Plateau as seen in Fig. 5.2 of Manabe *et al.* (1974). The above analysis suggests that the effect of the Tibetan Plateau is not merely the flow over mountains as parameterized in conventional linear theories. By comparing Fig. 5.4 and the lower portion of Fig. 5.3b, it is seen that the sinking motion occurs somewhere between the Siberian high and the Aleutian low. This means that the frictional convergence (Charney and Eliassen, 1949) which should occur in the low pressure area of the Ekman layer does not significantly affect the vertical velocity at 940 mb. This result is consistent with a theoretical model of Smagorinsky (1953) for stationary waves with large meridional width. It should also be noted that this sinking motion is associated with cold air (see Fig. 5.10 bottom), implying that available potential energy is being converted to kinetic energy.

In order to examine the detailed structure of stationary waves by spectral analysis, the meridional cross sections of the power spectra of stationary wavenumber 1, for geopotential height, zonal wind component,

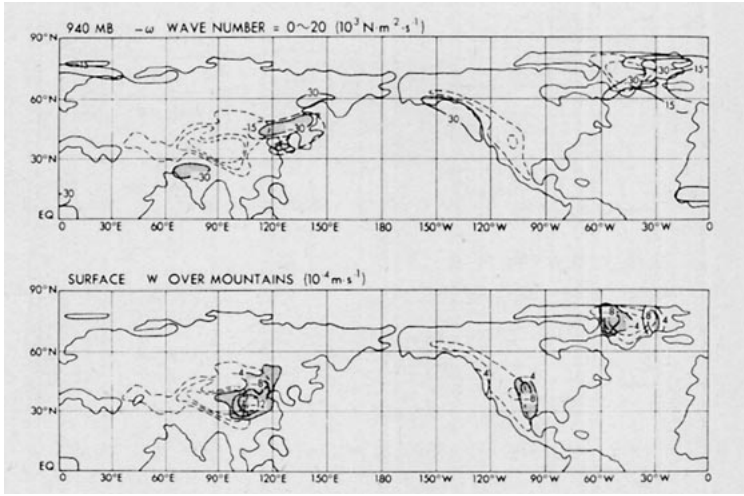

FIG. 5.4. Map of time-mean vertical pressure velocity ($-\omega$, top) in the model and topographically induced vertical velocity (w, bottom) adapted from Saltzman and Irsch (1972).

temperature and the vertical p-velocity are given in Fig. 5.5.

The geopotential height (Fig. 5.5a) of the stationary wave shows major maxima around 55°N, both in the troposphere and in the stratosphere. On the other hand, the major tropospheric maximum of the zonal compo-

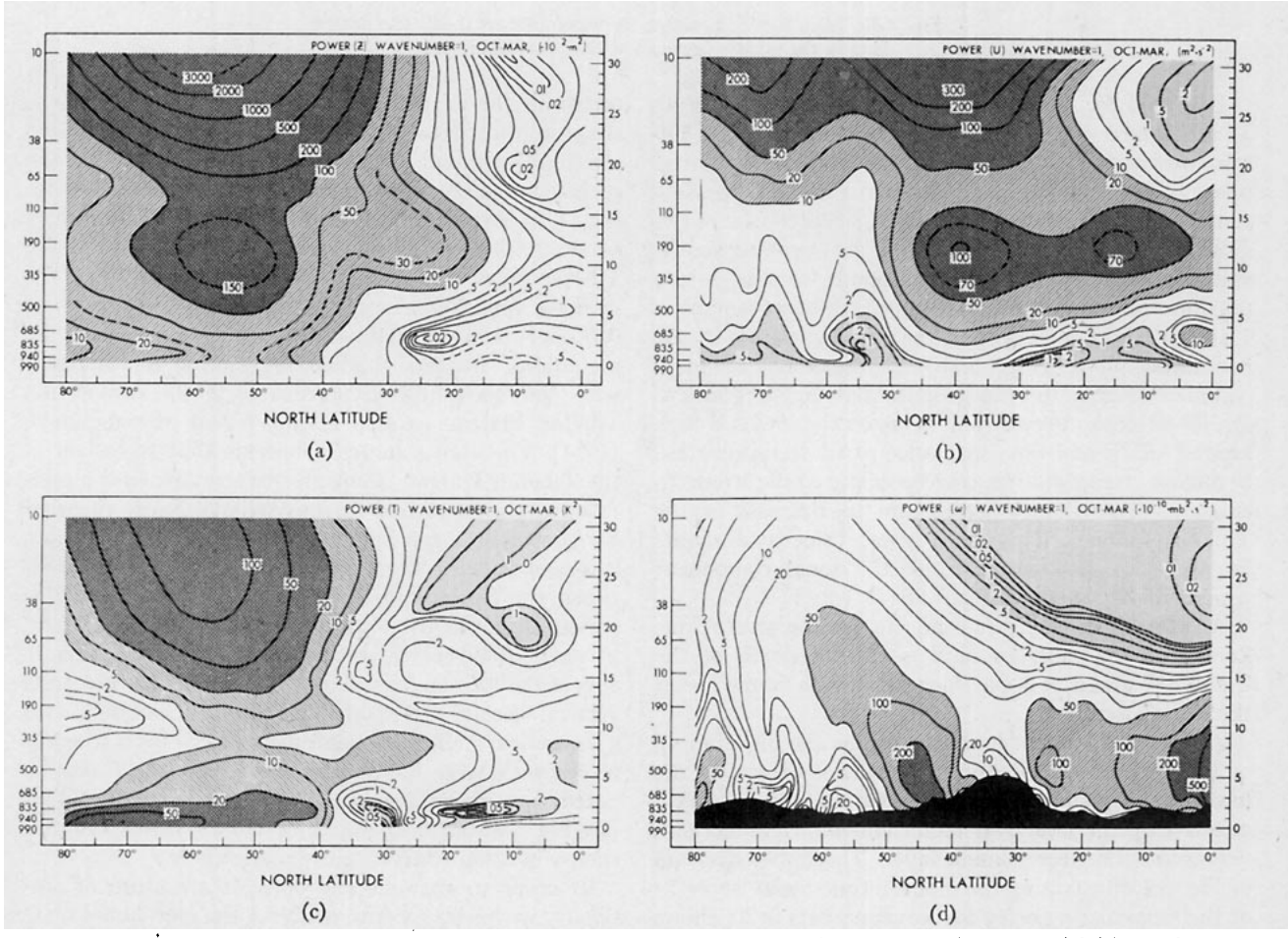

FIG. 5.5. Latitude-height sections of the power spectra of the stationary wave (wavenumber 1) geopotential (a), zonal component (b), temperature (c) and vertical pressure velocity with topography (maximum surface level) (d).

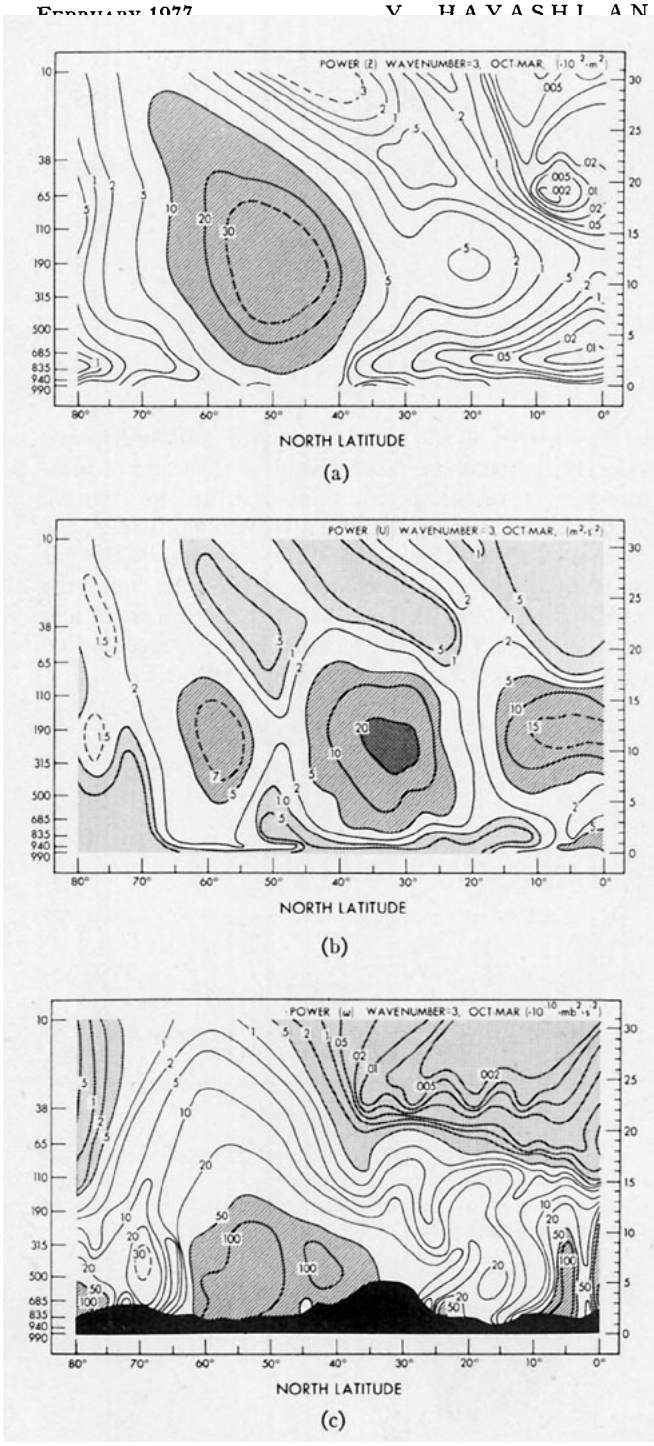

FIG. 5.6. As in Fig. 5.5 except for geopotential (a), zonal component (b) and vertical pressure velocity with topography (c) for wave number 3.

nent occurs at the latitude (30–40°N) of the Tibetan Plateau, indicating that the tropospheric stationary wave has more kinetic energy here. This large zonal component amplitude may be interpreted as a strengthening of the jet stream to the east of the Tibetan Plateau, as has been shown in Fig. 5.3b.

Fig. 5.5c shows that the temperature perturbation is large in mid-latitudes, while it is small in low latitudes in agreement with observations by Oort and Rasumusson (1964). This means that the tropospheric stationary waves corresponding to the Siberian high and the Aleutian low are associated with relatively large eddy available potential energy compared to that of the stationary waves appearing in the subtropical jet.

Fig. 5.5 shows that the vertical velocity associated with mid-latitude stationary waves attains its maximum to the north (~45°N) of the latitude of the Tibetan Plateau. The latitudinal maximum shifts poleward with height following the shifting of the maximum of westerly zonal flow presented in Fig. 3.1a.

The power spectra of stationary wavenumber 3 are presented in Fig. 5.6 for comparison. The power spectrum of geopotential height for wavenumber 3 (Fig. 5.6a) indicates only one maximum, at 50°N and 190 mb, and is smaller than that of wavenumber 1 by a factor of 5. However, the amplitude is in agreement with the observed amplitude of wavenumber 3 (see van Loon *et al.*, 1973). The power spectrum of the zonal component of wavenumber 3 (Fig. 5.6b) attains its maximum at 30°N, 190 mb where the subtropical jet appears.

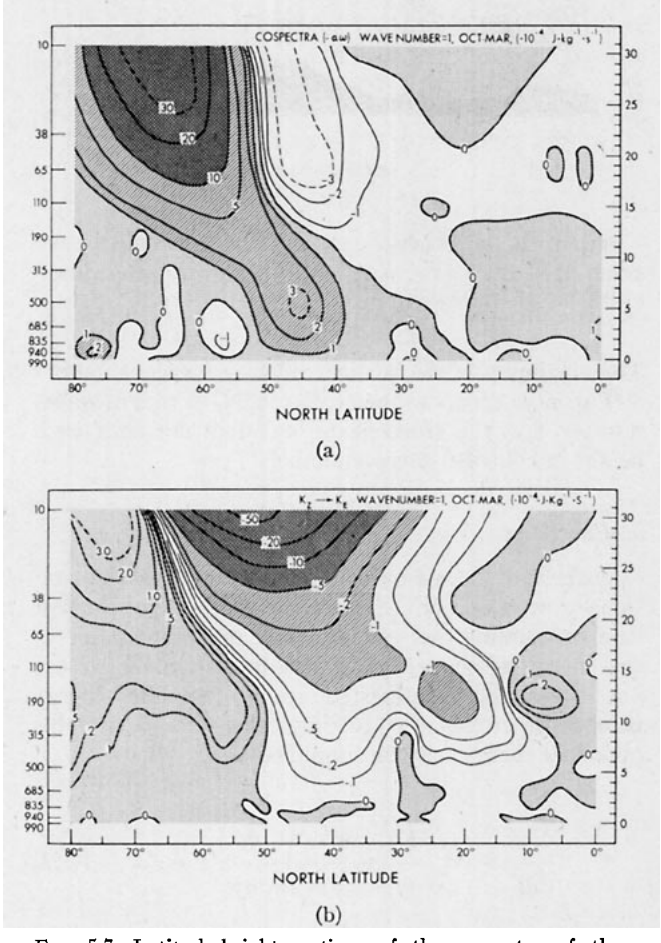

FIG. 5.7. Latitude-height sections of the cospectra of the stationary wave (wavenumber 1) eddy conversion (a) and horizontal barotropic conversion (b).

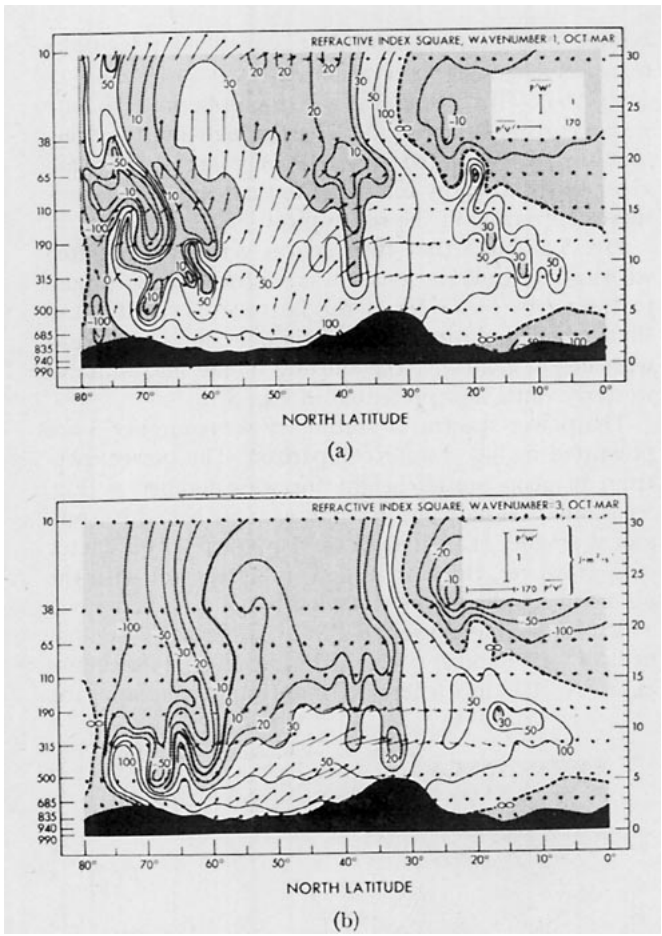

FIG. 5.8. Latitude-height sections of refractive index square and energy flux vector ($\overline{p'v'}$, $\overline{p'w'}$) for the stationary wave: wavenumber 1 (a), wavenumber 3 (b).

The maximum of the vertical velocity for wavenumber 3 (Fig. 5.6c) occurs to the north (55°N) of that of wavenumber 1 in the troposphere and does not shift with height in contrast to wavenumber 1.

b. Energetics

With the three-dimensional structure of the stationary waves described above, it would be of interest here to examine the sources, sinks and propagation of the energy associated with these waves. Since we are not particularly interested in a complete energy balance, equations of eddy kinetic energy and available potential energy may be simplified as

$$\frac{\partial \mathrm{KE}}{\partial t} = -\left(\frac{\partial \overline{\phi' v'}}{\partial y} + \frac{\partial \overline{\phi' \omega'}}{\partial p}\right) - \frac{\partial \bar{u}}{\partial y}\overline{u'v'} - \overline{\alpha'\omega'}, \tag{5.3}$$

$$\frac{\partial \mathrm{AE}}{\partial t} = -\frac{\partial \bar{\alpha}}{\sigma \partial y}\overline{v'\alpha'} + \overline{\alpha'\omega'} + \gamma \overline{\alpha' Q'}, \tag{5.4}$$

where

$$\mathrm{KE} \equiv \tfrac{1}{2}\overline{(u'^2 + v'^2)}, \tag{5.5}$$

$$\mathrm{AE} \equiv \frac{\overline{\alpha'^2}}{2\sigma}, \tag{5.6}$$

$$\sigma \equiv -\bar{\alpha}\frac{\partial \ln \bar{\Theta}}{\partial p}, \tag{5.7}$$

$$\gamma \equiv \frac{R}{c_p \sigma p}. \tag{5.8}$$

In the above u and v are eastward and northward velocity components, respectively, ω the vertical pressure velocity, α the specific volume, ϕ the geopotential, Q the heating rate, Θ the potential temperature, c_p the specific heat capacity at constant pressure, R the gas constant, p the vertical coordinate pressure and y the lateral coordinate. The overbar denotes the zonal and time average. The above energy terms are computed with corrections due to the sphericity of the earth.

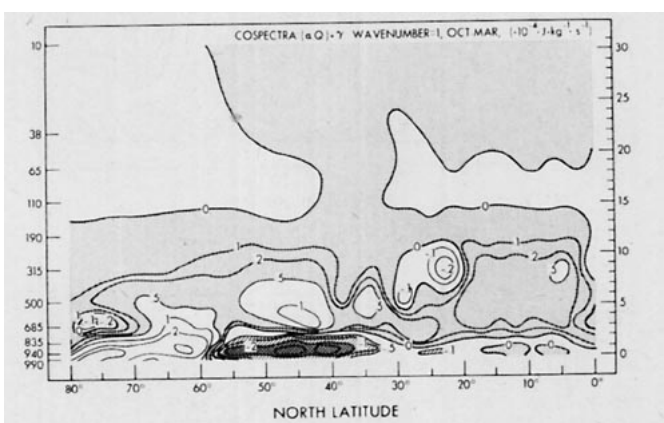

FIG. 5.9a. Latitude-height sections of the cospectra of the stationary wave (wavenumber 1) for generation of eddy available potential energy by diabatic heating (i.e., convective heating plus vertical diffusion of sensible heat).

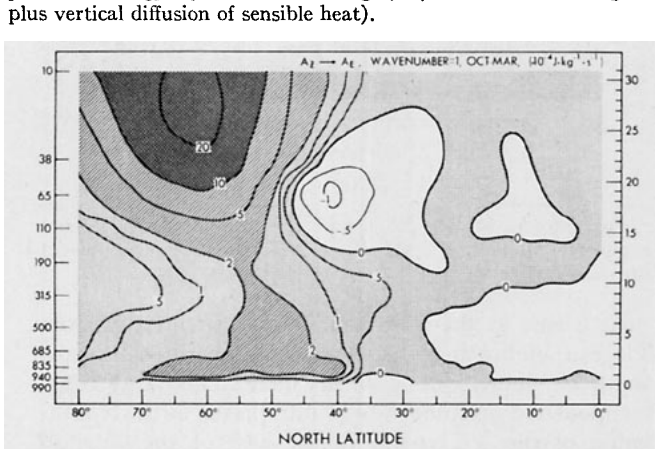

FIG. 5.9b. As in Fig. 5.9a except for conversion of zonal available potential energy into eddy available potential energy.

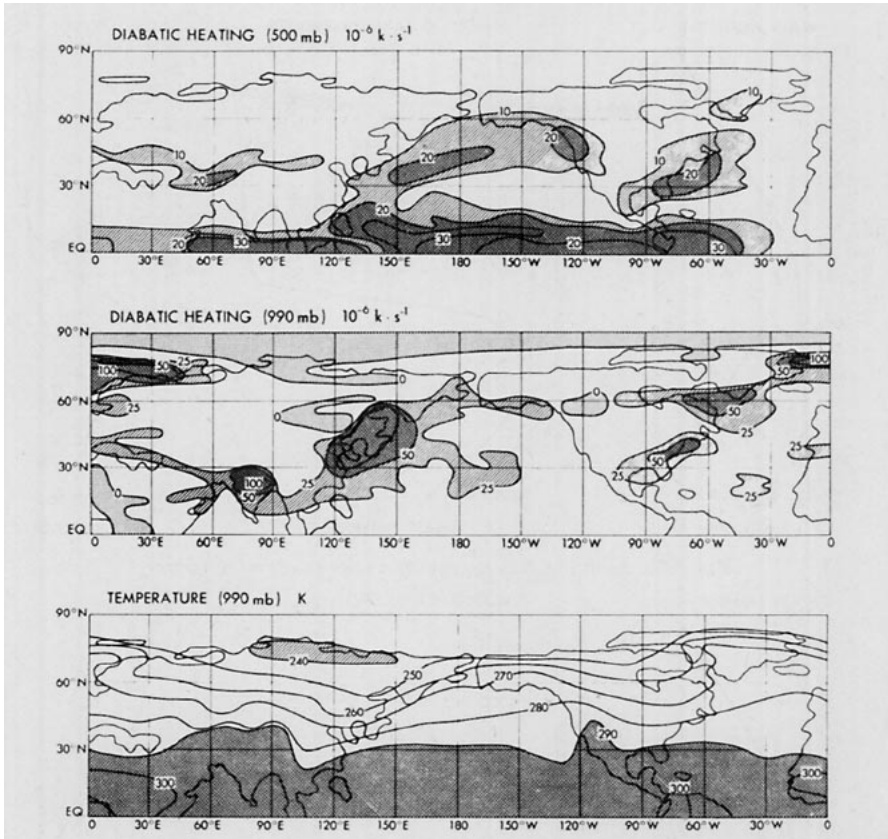

FIG. 5.10. Geographical distribution of the time-mean diabatic heating at 500 mb (top), 990 mb (middle) and the temperature at 990 mb (bottom).

The conversion of eddy available potential energy to eddy kinetic energy ($-\overline{\alpha'\omega'}$) for stationary wavenumber 1, shown in Fig. 5.7a, attains its tropospheric maximum at 40–50°N and its stratospheric maximum at 60–70°N. Although the stationary waves can be seen gaining energy from available potential energy, they

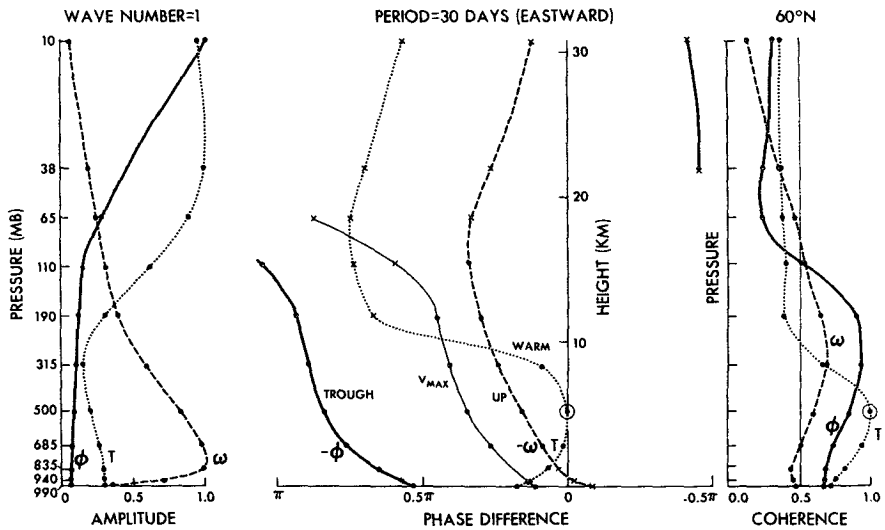

FIG. 6.1a. Vertical profile of normalized amplitude (left), phase difference (middle) and vertical coherence (right) with respect to temperature at 500 mb (circled). Phase difference associated with low coherence (<0.5) is indicated by cross. Wavenumber 1, period 30 days (eastward moving), 60°N.

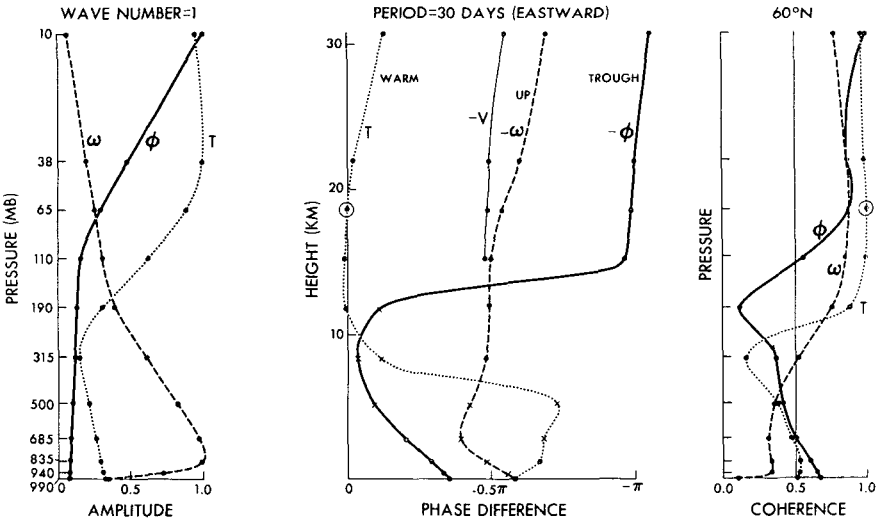

FIG. 6.1b. As in Fig. 6.1a except for a reference level of 65 mb.

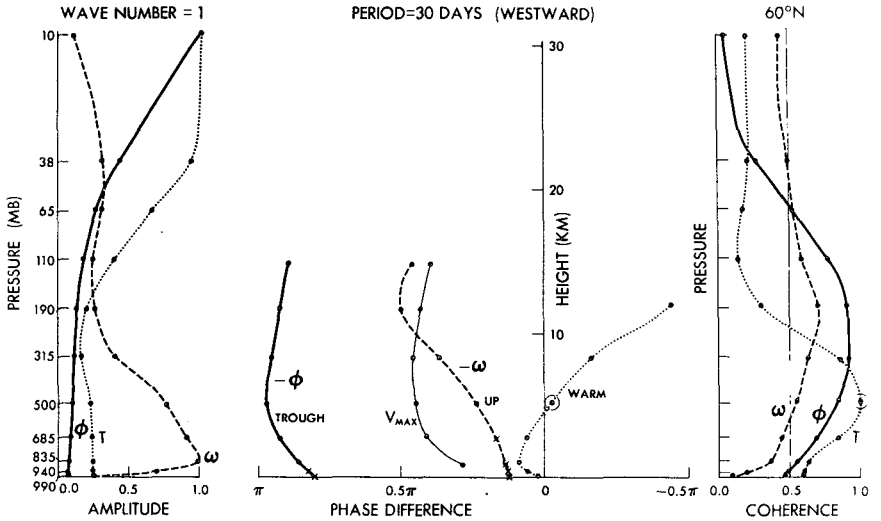

FIG. 6.2a. As in Fig. 6.1a except for westward moving ultra-long waves.

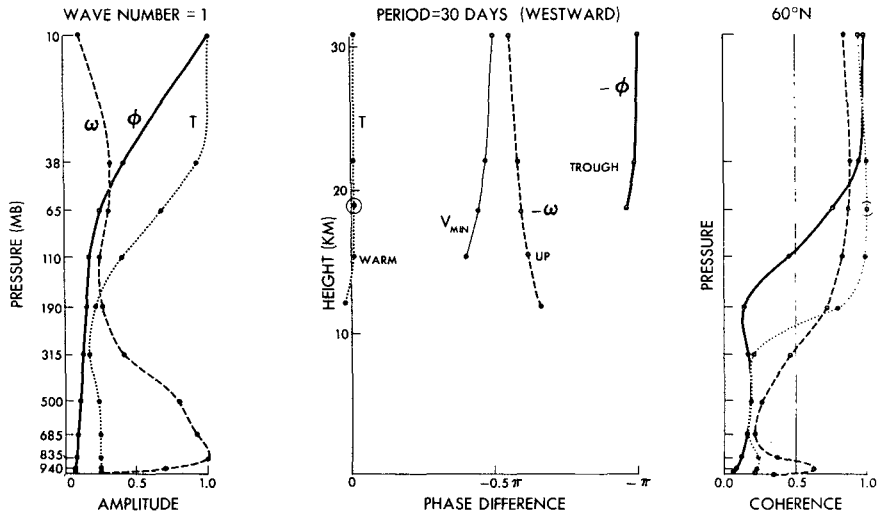

FIG. 6.2b. As in Fig. 6.2a except for a reference level of 65 mb.

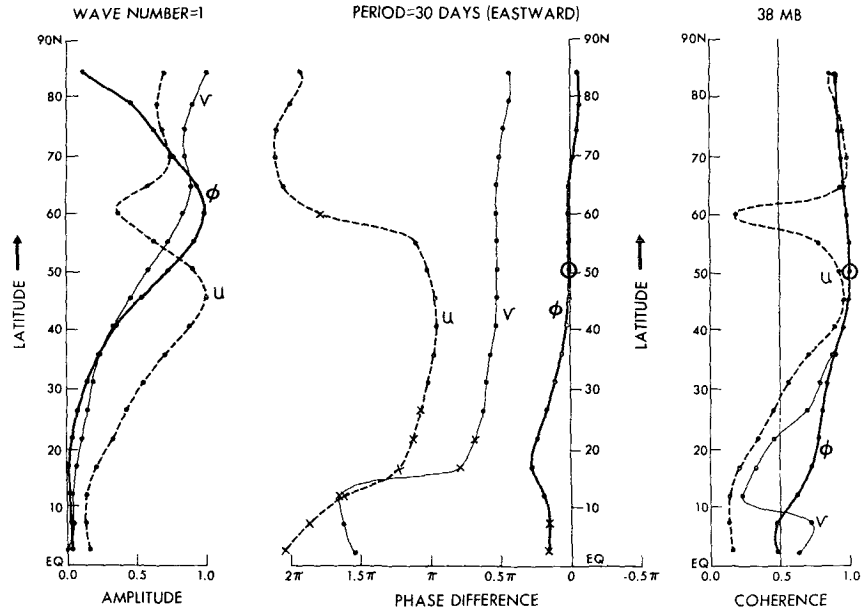

FIG. 6.3. Meridional profiles of normalized amplitude (left), meridional phase difference (middle) and meridional coherence (right) with respect to geopotential at 50°N (circled). Phase difference associated with low coherence is indicated by a cross. Wavenumer 1, period 30 days (eastward moving), 38 mb.

lose their eddy kinetic energy to zonal kinetic energy of the stratospheric and subtropical jets as is illustrated by Fig. 5.7b.

It will be of interest to examine how the wave energy flows in a meridional cross section. The energy is expected to flow from its source in such a way as to avoid the region of small refractive index square as demonstrated by Matsuno (1970). The refractive index square for isothermal atmospheres is given by Matsuno (1970) as

$$Q_m \equiv \frac{1}{\bar{\omega}\cos\theta}\frac{\partial \bar{q}}{\partial \theta} - \frac{m^2}{\cos^2\theta} - \frac{l^2\sin^2\theta}{4H_0^2}, \qquad (5.9)$$

where $\bar{\omega}$ is the angular speed of the basic zonal flow, θ is the latitude, $\bar{q}$ is the potential vorticity of the basic state and $\partial\bar{q}/\partial\theta$ involves the first and second derivative of zonal wind, and m is the zonal wavenumber.

Fig. 5.8a shows the refractive index square for wavenumber 1 computed from the model's zonal wind (Fig. 3.1a) and energy flux vector ($\overline{p'v'}$, $\overline{p'w'}$). It should be noted that the refractive index square becomes very small at 40°N and 20 km. The energy seems to flow toward the subtropical jet and the stratospheric jet avoiding this region. It should be mentioned that according to the theory by Charney and Drazin (1961), we should expect small refractive index square in the region of strong westerlies. However, it turns out that the refractive index square becomes large at the latitude of strong westerlies due to the large second derivative of the horizontal wind shear which is neglected by Charney and Drazin (1961).

The refractive index square and the energy flux vectors for wavenumber 3 are also presented in Fig. 5.8b for comparison. It is seen that the refractive index square is small in the stratosphere and the energy flow is confined in the troposphere. In this respect, this result is consistent with the theory by Charney and Drazin (1961) that waves with higher wavenumbers are trapped vertically.

The above energy flux suggests that the kinetic energy of the stationary wave in the subtropical jet is supplied by the energy flux from north of the latitude of the Tibetan Plateau rather than directly by the flow over the mountains. It should be noted that the eddy conversion within the subtropical jet is small[1] (Fig. 5.7a) and the wave loses its kinetic energy to the zonal mean kinetic energy (Fig. 5.7b).

Since stationary waves were generated particularly in the lower troposphere by the regional difference of the diabatic heating in the land-sea model without mountains (Manabe and Terpstra, 1974), it is of interest here to examine the effect of such heating in the present study. Fig. 5.9a shows that eddy available potential energy is generated by diabatic heating while it is destroyed near the surface between 35°N and 55°N. The diabatic heating in the mid-troposphere is mainly the result of moist convective heating, while that near the surface is mainly due to the sensible heat flux from the surface. Although the eddy available potential energy is destroyed near the surface, it is converted

[1] This eddy conversion is much smaller than the convergence of the energy flux [see Figs. 9.3 and 9.4 in Manabe and Mahlman (1976)].

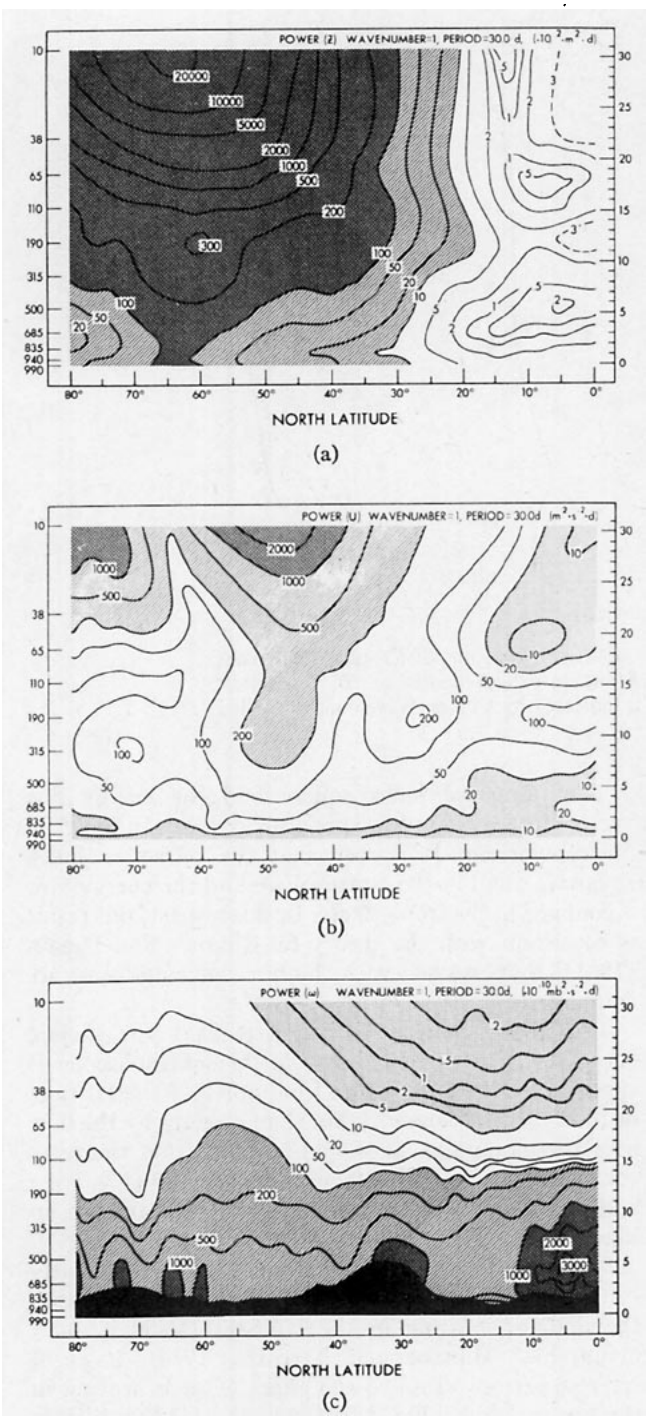

FIG. 6.4. Latitude-height sections of power spectrum density of eastward moving waves (wavenumber 1, period 30 days) for geopotential (a), zonal component (b) and vertical pressure velocity (c).

from the zonal available potential energy as seen in Fig. 5.9b. This suggests that the effect of the sensible heat flux at latitudes 35–55°N is to trigger stationary waves which actually derive their energy from the zonal available potential energy and the convective heating in the mid-troposphere. This interpretation is consistent with observational studies by Brown (1964) and Holopainen (1970), who showed that diabatic heating destroys the available potential energy during the winter season. On the other hand, between 55-80°N diabatic heating actually generates the eddy available potential energy.

The geographical distribution of the diabatic heating is shown in Fig. 5.10 in order to interpret the above spectral analysis. The diabatic heating at 500 mb (upper diagram) shows maxima over the Pacific and the western Atlantic. The diabatic heating at 990 mb (middle diagram) attains its maxima over northeast China, near Japan, where the temperature (bottom diagram) is relatively cold and also over the Gulf Stream in the North Atlantic.

6. Analysis of transient ultra-long waves

a. Three-dimensional structure

The vertical structure of the eastward moving ultra-long wave at 60°N is illustrated by Fig. 6.1a, b. The phase lines shown in Fig. 6.1a tilt westward with height in the lower troposphere in agreement with the observed eastward moving ultra-long waves (Pratt and Wallace, 1976). On the other hand, the phase lines tilt slightly eastward with height in the stratosphere. Since the vertical coherence with respect to temperature at the 500 mb level drops in the stratosphere, the vertical phase difference in the stratosphere in Fig. 6.1a may not be meaningful. In order to confirm this eastward tilt, Fig. 6.1b is presented. This figure is similar to that of Fig. 6.1a except that the vertical coherence and phase difference are measured with respect to the 65 mb level, resulting in a high vertical coherence in the stratosphere.

Although westward moving components of transient ultra-long waves are weak and are not associated with a frequency spectral peak (Fig. 4.6), it is of interest to compare their vertical structure with that of eastward moving components. This westward moving component is partly due to the standing wave oscillations which are composed of both westward and eastward components, as will be seen in Fig. 6.5. From Figs. 6.2a, and 6.2b, it can be seen that the vertical profiles of the normalized amplitude are similar to those of the eastward moving ultra-long wave. However, the vertical tilt of the phase lines is smaller than that of the eastward moving wave. According to Pratt and Wallace (1976), the observed westward moving ultra-long wave exhibits little vertical tilt in the troposphere. This result is also consistent with the theoretical studies by Wiin-Nielsen (1971a,b), that ultra-long waves with lower vertical mode are associated with larger westward phase velocity.

The meridional structure of the stratospheric (38 mb) eastward moving ultra-long wave is shown by Fig. 6.3. The north–south profiles of the amplitudes of the zonal and meridional wind components along with geopotential reveal that these waves take the form of eddies

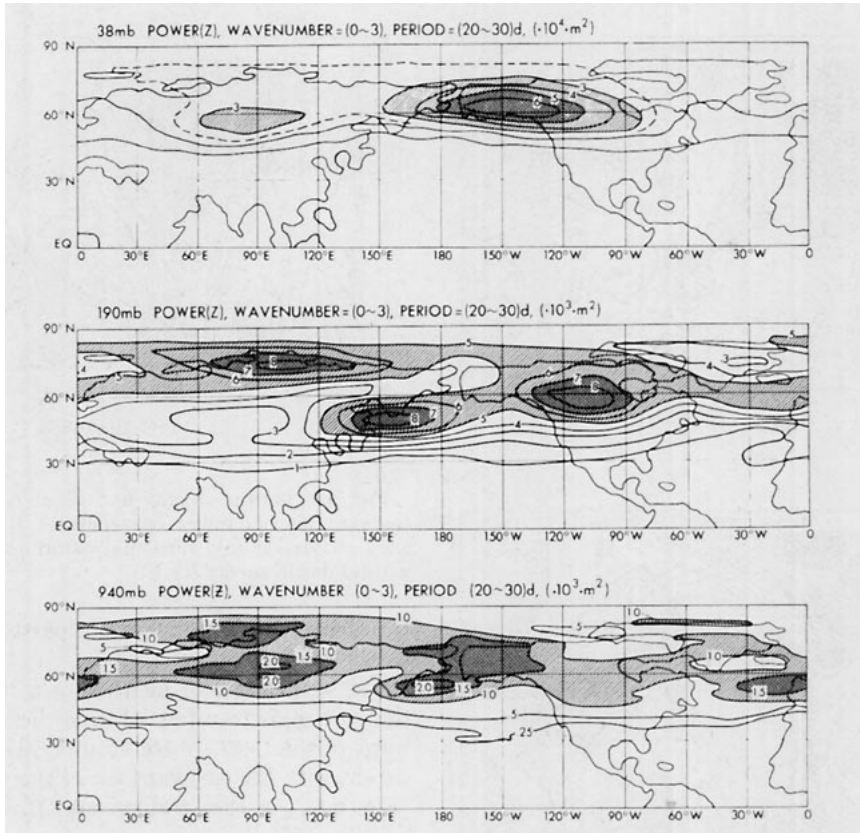

FIG. 6.5. Geographical distributions of time-power spectra (integrated over periods 20–30 days) of wavenumber filtered geopotential height (wavenumber 0–3) at 38 mb (top), 190 mb (middle), 940 mb (bottom).

centered at 60°N and tilt slightly from southeast to northwest in the low and high latitudes.

The latitude-height distribution of the power spectrum of the eastward moving ultra-long wave is presented in Fig. 6.4. The geopotential (Fig. 6.4a) looks similar to that of the stationary ultra-long wave (Fig. 5.5a) except that the tropospheric maximum is at 60°N, i.e., 5° north of that of the stationary wave. This difference is more apparent in the zonal component of the wind (Fig. 6.4b) which shows a maximum occurring at 40–50°N, i.e., 10° north of that of the stationary wave (Fig. 5.5b).

Fig. 6.4c shows that the power spectrum of the vertical p-velocity attains its maximum around 60°N in the stratosphere. Unlike the stationary ultra-long wave (Fig. 5.5d), the vertical p-velocity in the troposphere is not particularly large to the north of the Tibetan Plateau.

The horizontal distribution of the time-power spectra (integrated over periods of 20–30 days) of geopotential height, consisting of wavenumbers 0–3, is given in Fig. 6.5. The upper diagram (38 mb) shows that the maximum amplitude occurs over Alaska (150°W) where the stationary high pressure is situated (see Fig. 5.3a). A time-longitude section at 38 mb (not illustrated) shows that wave amplitudes pulsate like standing wave oscillations at this longitude. These standing wave oscillations are composed of eastward and westward moving components which are coherent with each other (see Hayashi, 1977).

On the other hand, the middle diagram (190 mb) indicates that three maxima over northern Russia, Japan and Canada do not coincide with the stationary high or low in Fig. 5.3a. In Hayashi (1977) it is shown that wavenumber 1 at 60°N, 190 mb travels back and forth rather than pulsates like standing wave oscillations. The lower diagram (940 mb) reveals two maxima corresponding to the pulsation of the Siberian high and Aleutian low in Fig. 5.3a.

b. Energetics

Fig. 6.6a shows that for the eastward moving ultra-long waves, the baroclinic conversion $(-\overline{\alpha'\omega'}>0)$ from eddy available potential energy to eddy kinetic energy occurs in the troposphere. These eastward moving waves have a steering level in the troposphere consistent with baroclinically unstable waves. On the other hand, Fig. 6.6b shows a large barotropic conversion from zonal to eddy kinetic energy occurring in the stratosphere where unrealistically strong horizontal shear exists. This feature is consistent with the linear baro-

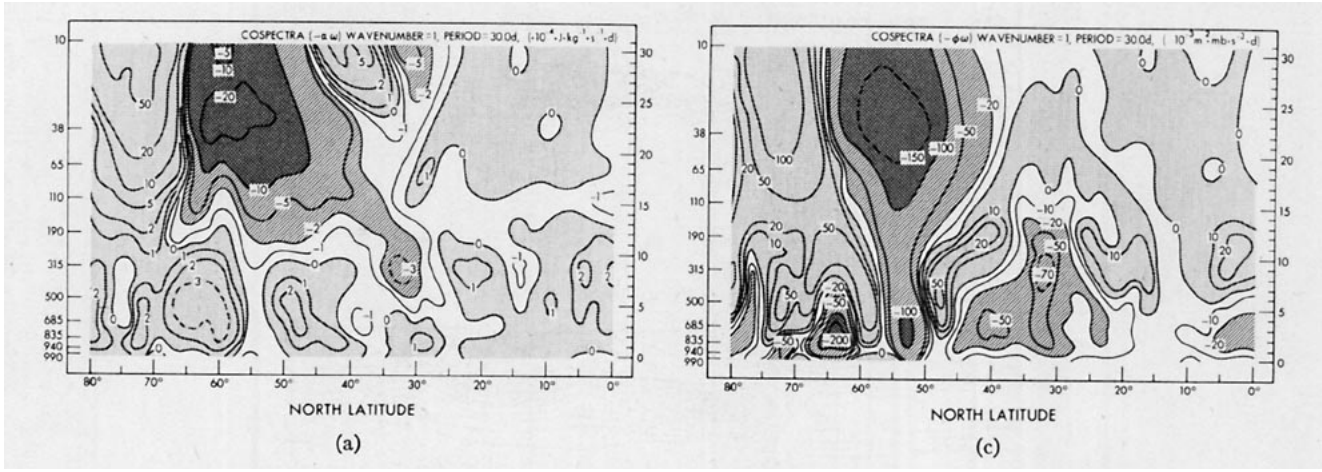

FIG. 6.6. Latitude-height sections of cospectrum density of eastward moving waves (wavenumber 1, period 30 days) for eddy conversion (a), horizontal barotropic conversion (b) and vertical flux of energy (c).

tropic instability of the present model examined by Gall (1976a). There is also the possibility of nonlinear energy transfer from stationary waves, since the transient ultra-long waves are partly due to the pulsation of standing waves.

The vertical flux of energy shown in Fig. 6.6c indicates that energy is transported from the stratosphere downward to the troposphere around 50–60°N. This is consistent with the eastward tilt of the vertical phase lines (Fig. 6.1b) in the stratosphere. However, this feature may be unrealistic.

7. Analysis of transient long waves

a. Three-dimensional structure

Fig. 7.1 shows the vertical structure of the transient long wave with wavenumber 5 [a period of 12 days (Fig. 7.1a)] and with wavenumber 7 [a period of 3.75 days (Fig. 7.1b)]. Both the figures reveal that the

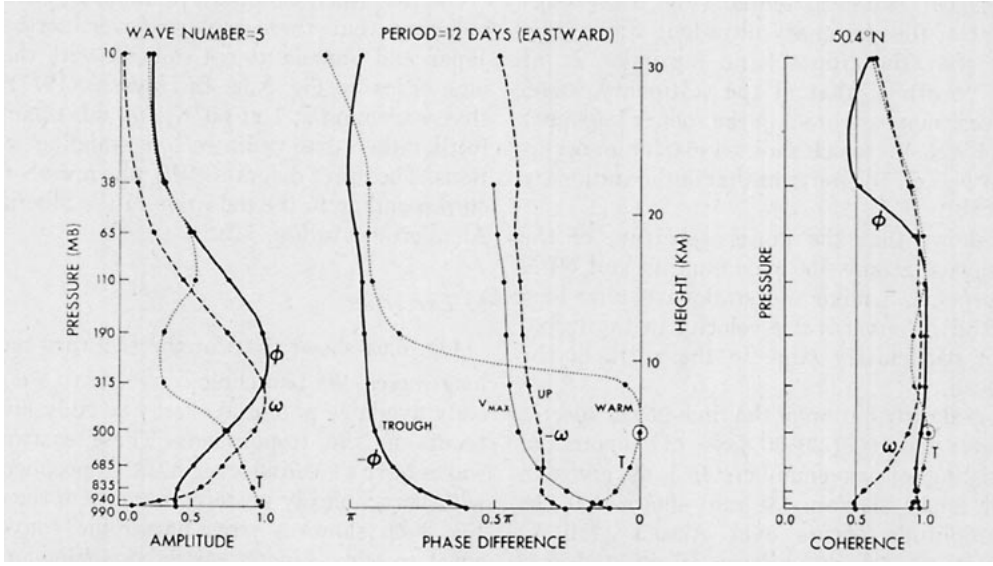

FIG. 7.1a. Vertical profile of normalized amplitude (left), vertical phase difference (middle) and vertical coherence (right) with respect to the temperature at 500 mb (circled). Wavenumber 5, period 12 days (eastward moving), 50.4°N.

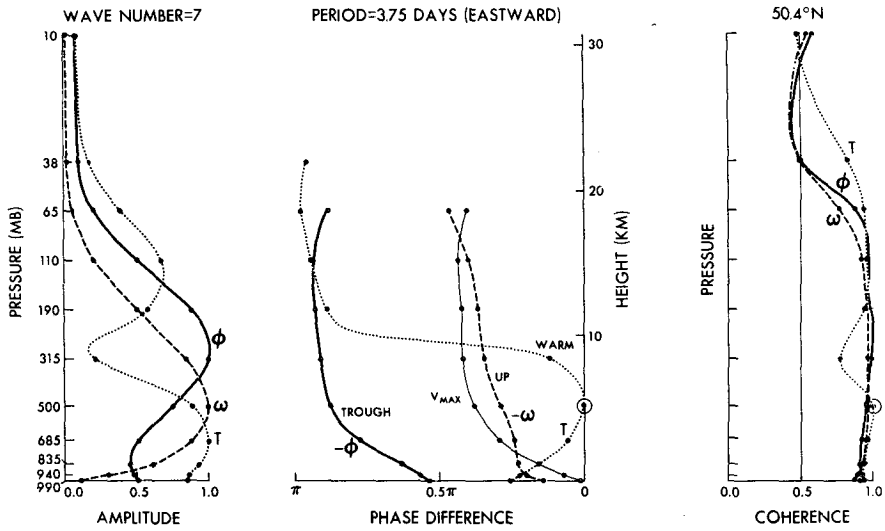

FIG. 7.1b. As in Fig. 7.1a except for wavenumber 7, period 3.75 days.

amplitude of the geopotential attains its maximum around 300 mb, while the amplitude of the temperature has its maximum near the surface. For the lower troposphere, the trough line tilts westward with height, while the temperature tilts eastward and exhibits a 180° phase jump around 300 mb. This is consistent with the linear theory of Kuo (1952) and the spectral analysis by Nitta *et al.* (1973) and Hartmann (1974).

One can also note that upward motion occurs to the east of the trough even at 990 mb where frictional convergence takes place. Barcilion (1964) and Williams and Robinson (1974) theoretically studied the effect of Ekman pumping on baroclinic waves. According to Williams and Robinson, upward motion occurs at the trough near the surface. This discrepancy with the general circulation model may be due to the large surface friction in their model which is designed to simulate laboratory annulus experiments.

In a recent study, Gall (1976a) examined the growth of long waves by using a linear model with the same static stability and wind shear as that of the general circulation model used in the present study. Fig. 7.2 displays the vertical structure of Gall's wavenumber 7 for comparison. His waves are similar to those in Fig. 7.1b except that the temperature and vertical velocity are more in phase and that the geopotential attains its maximum near the surface rather than around 300 mb where it exhibits a secondary maximum. Gall (1976b) further demonstrated by a zonal wave interaction model that the amplitude aloft becomes

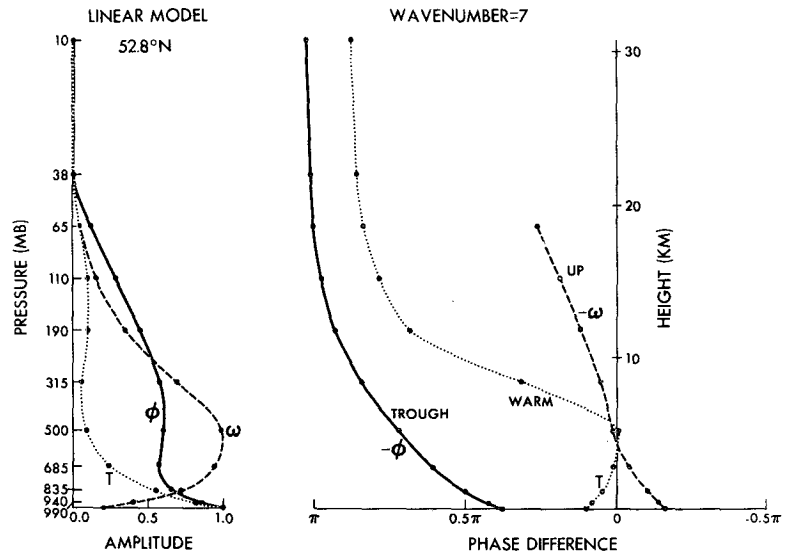

FIG. 7.2. Vertical profile of normalized amplitude (left) and phase difference (right) of a linear experiment of a general circulation model (after Gall, 1976a).

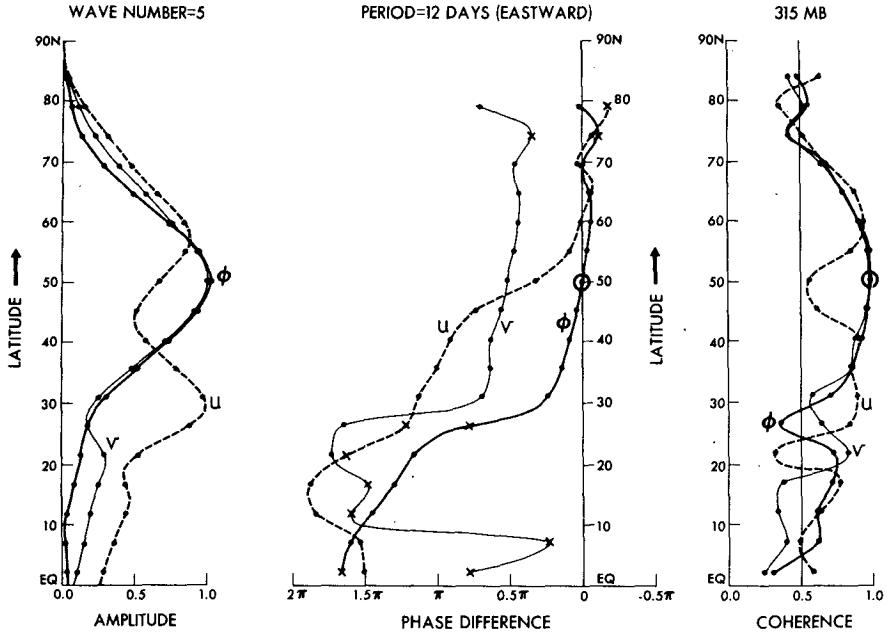

FIG. 7.3. Meridional profiles of normalized amplitude (left), meridional phase difference (middle) and meridional coherence (right) with respect to the temperature at 50°N (circled). Phase difference associated with low coherence (<0.5) is indicated by a cross. Wavenumber 5, period 12 days (eastward moving), 315 mb.

largest when the wave reaches its mature stage. The present spectral analysis results seem to be contributed to mostly by mature stage cyclones which have a large amplitude aloft.

In Fig. 7.3, we show the latitudinal distributions of the amplitude, phase and coherence at 315 mb of the models geopotential and wind components for wavenumber 5 (eastward moving, 12-day period). Examination of the left-hand side of Fig. 7.3 reveals that the geopotential is confined to mid-latitudes, with the maximum meridional wind and geopotential amplitudes occurring at 50°N, where westerlies attain their latitudinal maximum in the lower troposphere (see Fig. 3.1a). This feature is consistent with the theories of the meridional scale of baroclinic unstable waves discussed by Stone (1969, 1975), Simmons (1974b, 1975) and Gent (1974, 1975).

The right-hand side of Fig. 7.3, where the geopotential at 50.4°N was used as a reference, shows a large horizontal coherence between 30° and 50°N. Here, the zonal component is 90° out of phase with the meridional component and undergoes a 180° phase shift across 50°N indicating that those waves take the form of a vortex. The tilt in the phase line from southwest to the northeast in the mid-latitudes indicates a poleward momentum flux.

In Fig. 7.4 the latitude-height distributions of several variables of the model's long wave are shown. It is seen that the power spectrum of the geopotential (Fig. 7.4a) attains its maximum around 50°N and 300 mb. The power spectrum of the temperature (Fig. 7.4b) attains a primary maximum at the surface between 45° and 60°N and a secondary maximum at 100 mb and 45°N. The vertical p-velocity (Fig. 7.4c) shows maxima at 500 mb between 35° and 55°N. It should be mentioned here that wavenumber 7 (not illustrated) has a similar meridional-vertical structure.

In order to examine the regional variation of the intensity of long waves, the horizontal distribution at 500 mb of the time-power spectra (integrated over periods of 3–20 days) of the meridional component, consisting of wavenumbers 4–10, is presented in Fig. 7.5 (top). The maxima of the power spectra are found to occur over the Pacific and the Atlantic. These maxima are situated to the east of the strong north–south temperature gradient (Fig. 7.5 bottom) on the leeward side of the Tibetan Plateau and Rocky Mountains.

This result may be interpreted to mean that cyclones are generated on the leeward side of the Tibetan Plateau and Rocky Mountains where the baroclinicity is large and then develop as they move eastward. This interpretation is consistent with Petterssen (1956) who showed that there is a significant increase in the frequency of cyclogenesis on the leeward side of the Tibetan Plateau and Rocky Mountains. The present result is also in agreement with the statistical analysis of observed data by Blackmon (1976). This regional variation of amplitude may explain why Julian (1971) did not find a significant frequency spectral peak at Columbia, Mo. (39°N, 92°W), while Hartmann (1974) found a rather significant peak over the Atlantic (53°N, 35°W).

b. Energetics

Fig. 7.6a shows that the baroclinic conversion $(-\overline{\alpha'\omega'})$ attains its maximum below 500 mb near 50°N. The barotropic conversion $[-(\partial\bar{u}/\partial y)\overline{u'v'}]$ presented in Fig. 7.6b is small compared to the baroclinic conversion. It should be noted that the wave loses its energy to zonal kinetic energy to the north (35–45°N) of the latitude of the subtropical jet.

The vertical energy flux $(-\overline{\phi'\omega'})$ shown in Fig. 7.6c reveals that energy is transported upward between 45–60°N. This energy flux is important in maintaining the kinetic energy maximum at 300 mb.

Fig. 7.6d shows that available potential energy is generated also by the diabatic heating in the mid-troposphere at 50–60°N as simulated by Manabe *et al.* (1970), while it is being destroyed near the surface.

Fig. 7.7 shows the geographical distribution of the local generation of the eddy available potential energy by the baroclinic process (top) and the diabatic heating (bottom) for long waves. Here the overbar in the energy equation (5.4) means the time average only. It is seen that eddy available potential energy is generated not only by the baroclinic process but also by convective heating, particularly over the Pacific and Atlantic.

8. Conclusions

Based on a space-time cross spectral analysis of mid-latitude disturbances in the Northern Hemisphere, simulated by a global general circulation model during the period October through March, the following main conclusions have been made.

a. Stationary ultra-long waves

1) The stratospheric stationary waves attain their maximum amplitude in geopotential at the latitude of the maximum westerlies in agreement with observations, although their amplitude is too large. The tropospheric stationary waves corresponding to the Siberian high and the Aleutian low are characterized by relatively large available potential energy. On the other hand, a kinetic energy maximum occurs at 30–40°N, corresponding to the strengthening of the subtropical jet to the east of the Tibetan Plateau.

2) The wave energy flows upward and equatorward from the region of maximum energy conversion which occurs to the north of the latitude of the Tibetan Plateau. It avoids the region of low refractive index at 20 km and 40°N. The tropospheric stationary waves in the subtropical jet receive kinetic energy from this energy flow and lose it to the mean flow.

3) The eddy available potential energy of the tropospheric stationary wave is mainly converted from zonal available potential energy and is partly generated by convective heating. However, it is destroyed by the sensible heat flux from the surface particularly over northeastern China where the temperature is relatively low.

4) The sinking motion associated with the tropospheric stationary wave occurs somewhere between the Siberian high and Aleutian low, while rising motion occurs to the east of the Aleutian high. However, this

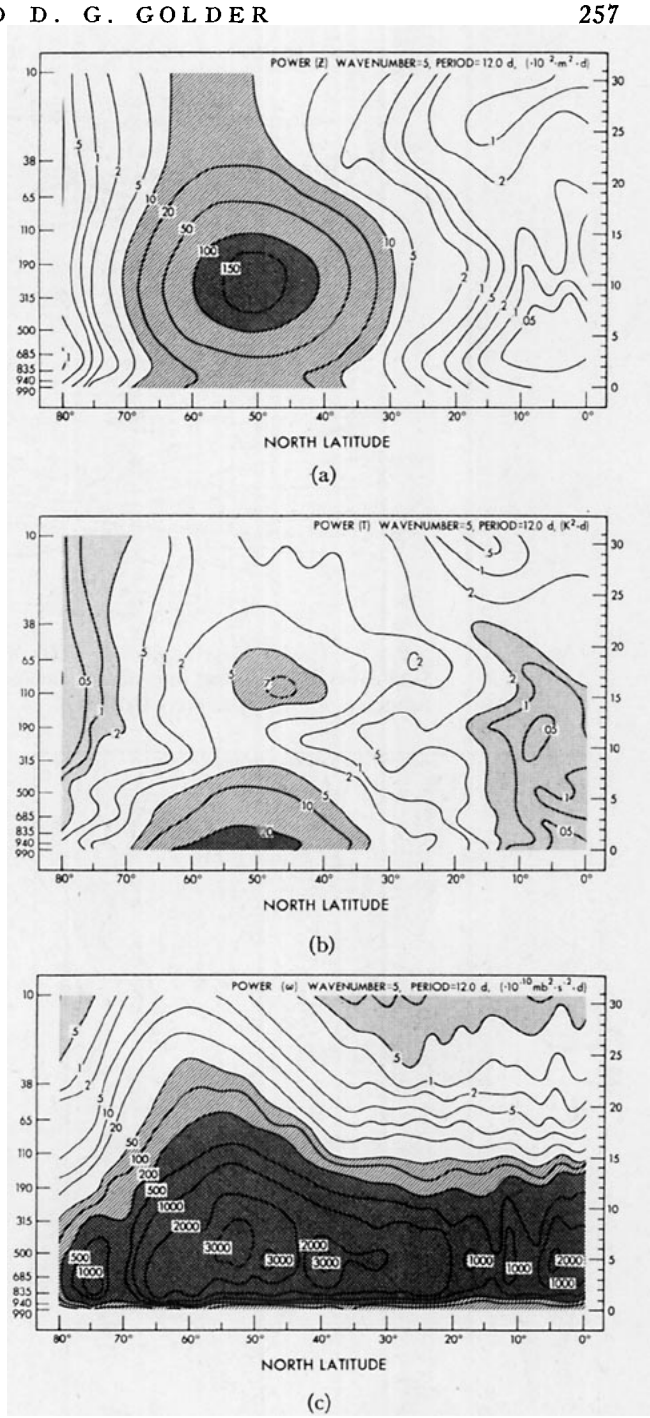

FIG. 7.4. Latitude-height sections of power spectrum density of eastward moving waves (wavenumber 5, period 12 days) for geopotential (a), temperature (b) and vertical pressure velocity (c).

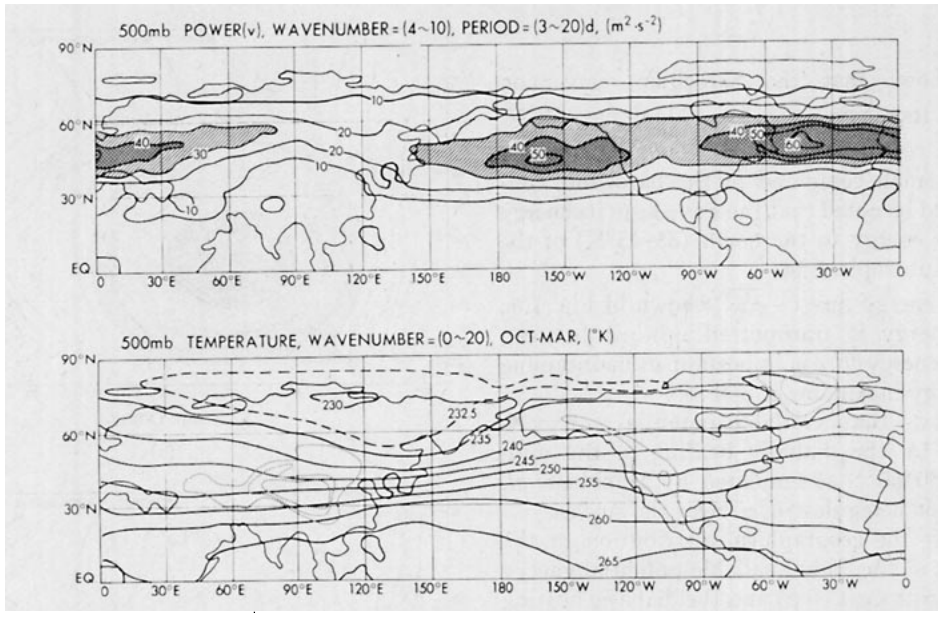

FIG. 7.5. Geographical distribution (500 mb) of time-power spectra (integrated over periods 3–20 days) of meridional component composed of wavenumbers 4–10 (top) and time-mean temperature with topography (bottom).

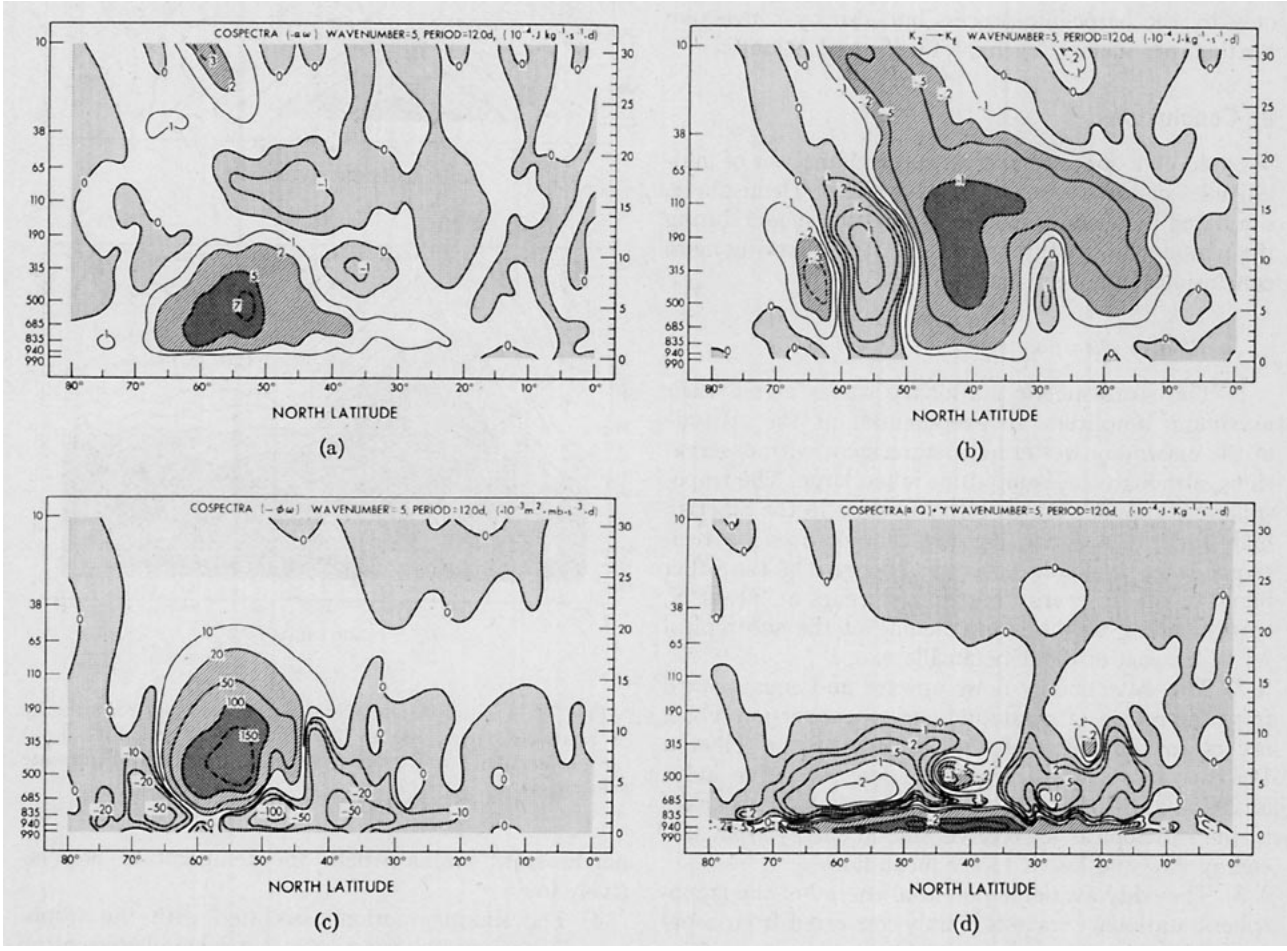

FIG. 7.6. Latitude-height sections of cospectrum density of eastward moving waves (wavenumber 5, period 12 days) for eddy conversion (a), horizontal barotropic conversion (b), vertical flux of energy (c) and generation of eddy available potential energy by diabatic heating (d).

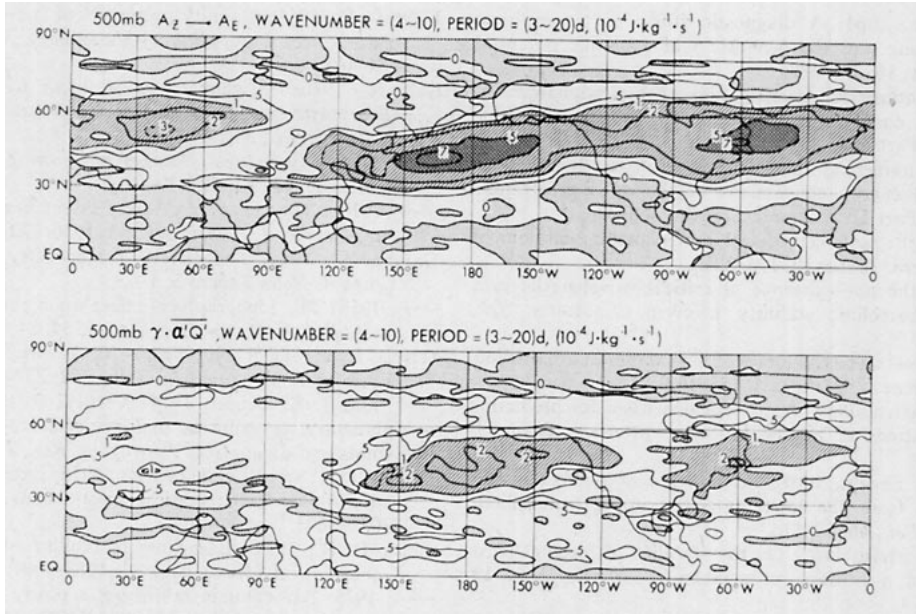

FIG. 7.7. Geographical distribution (500 mb) of time spectra (integrated over periods 3–20 days) of waves consisting of wavenumbers (4–10). Baroclinic conversion (top), generation of eddy available potential energy by diabatic heating (bottom).

sinking motion does not correspond to the flow over mountains or the Ekman pumping.

b. Transient ultra-long waves

1) The transient ultra-long waves (wavenumbers 1–3, period 20–60 days) are too weak in the troposphere and are associated with more eastward moving components than westward moving components contrary to those observed in the troposphere. They are partly due to the pulsation of standing waves.

2) The vertical phase lines tilt westward with height in the troposphere and slightly eastward in the stratosphere. The vertical tilt of the eastward moving component is larger than that of the westward moving component.

3) These waves derive their energy from the available potential energy in the troposphere and from the zonal kinetic energy in the stratosphere.

c. Transient long waves

1) The long waves are associated with two major spectral peaks, at wavenumber 5 (period of 12 days) corresponding to strong cyclones and at wavenumber 7 (period of 4 days) corresponding to weak cyclones.

2) The maximum kinetic energy occurs around 50°N at 300 mb in agreement with observations, while a linear theory predicts a kinetic energy maximum near the surface.

3) The kinetic energy maximum occurs to the east of the region of strong north–south temperature gradient found to the east of the Tibetan Plateau and Rocky Mountains. The eddy available potential energy is partly generated by convective heating over the Pacific and Atlantic.

4) The long waves lose their kinetic energy to the zonal kinetic energy to the north of the latitudes of the subtropical jet.

Acknowledgments. We wish to thank Dr. S. Manabe for his helpful suggestions and comments throughout this work. Valuable criticisms on the original manuscript were offered by Drs. K. Miyakoda and J. D. Mahlman. We are also grateful to Dr. J. Smagorinsky for his interest and encouragement. Thanks are extended to Mr. E. Green and Mrs. H. Kaufman for technical assistance, Mr. P. G. Tunison for drafting, Mr. J. N. Conner for photographing and Mrs. E. Thompson for typing the manuscript.

REFERENCES

Arai, Y., 1965: A statistical study of planetary waves. *J. Meteor. Soc. Japan*, **43**, 42–51.

——, 1971: A statistical study of ultra-long waves. *J. Meteor. Soc. Japan*, **48**, 469–478.

——, 1973: On the movement of planetary waves in wavenumber-period space. *J. Meteor. Soc. Japan*, **51**, 230–243.

Barcilion, V., 1964: Role of the Ekman layers in the stability of the symmetric regimes obtained in a rotating annulus. *J. Atmos. Sci.*, **21**, 291–299.

Bjerknes, J., and J. Holmboe, 1944: On the theory of cyclones. *J. Meteor.*, **1**, 1–22.

Blackmon, M. L., 1976: A climatological spectral study of the 500 mb geopotential height of the Northern Hemisphere. *J. Atmos. Sci.*, **33**, 1607–1623.

Bolin, B., 1950: On the influence of the earth's orography on the general character of the westerlies. *Tellus*, **2**, 184–195.

Bradley, J. H. S., and A. Wiin-Nielsen, 1968: On the transient part of the atmospheric planetary waves. *Tellus*, **20**, 533–544.

Brown, J. A., Jr., 1964: A diagnostic study of tropospheric diabatic heating and the generation of available potential energy. *Tellus*, **16**, 371–388.

——, 1969a: A numerical investigation of hydrodynamic instability and energy conversions in the quasi-geostrophic atmosphere, Part I. *J. Atmos. Sci.*, **26**, 352–365.

——, 1969b: A numerical investigation of hydrodynamic instability and energy conversions in the quasi-geostrophic atmosphere, Part II. *J. Atmos. Sci.*, **26**, 366–375.

Burger, A. P., 1958: Scale consideration of planetary motions of the atmosphere. *Tellus*, **10**, 195–205.

——, 1962: On the non-existence of critical wavelengths in a continuous baroclinic stability problem. *J. Atmos. Sci.*, **19**, 31–38.

Charney, J. G., 1947: The dynamics of long waves in a baroclinic westerly current. *J. Meteor.*, **4**, 135–162.

——, and A. Eliassen, 1949: A numerical method for predicting the perturbations of middle latitude westerlies. *Tellus*, **1**, 38–54.

——, and P. G. Drazin, 1961: Propagation of planetary-scale disturbances from the lower into the upper atmosphere. *J. Geophys. Res.*, **66**, 83–110.

——, and M. E. Stern, 1962: On the stability of internal baroclinic jets in a rotating atmosphere. *J. Atmos. Sci.*, **19**, 159–172.

——, and J. Pedlosky, 1963: On the trapping of unstable planetary waves in the atmosphere. *J. Geophys. Res.*, **68**, 6441–6442.

Clark, J. H. E., 1972: The vertical propagation of forced atmospheric planetary waves. *J. Atmos. Sci.*, **29**, 1430–1451.

Deland, R. J., 1964: Traveling planetary waves. *Tellus*, **16**, 271–273.

——, 1965a: Some observations of the behavior of spherical harmonic waves. *Mon. Wea. Rev.*, **93**, 307–312.

——, 1965b: On the scale analysis of traveling planetary waves. *Mon. Wea. Rev.*, **95**, 21–31.

——, 1972: On the spectral analysis of traveling waves. *J. Meteor. Soc. Japan*, **50**, 104–109.

——, 1973a: Spectral analysis of traveling planetary scale waves: Vertical structure in middle latitudes of Northern Hemisphere. *Tellus*, **25**, 356–373.

——, 1973b: Analysis of Nimbus 3 SIRS radiance data: Traveling planetary-scale waves in the stratospheric temperature field. *Mon. Wea. Rev.*, **101**, 132–140.

——, and Y. J. Lin, 1967: On the movement and prediction of traveling planetary-scale waves. *Mon. Wea. Rev.*, **95**, 21–31.

——, and K. W. Johnson, 1968: A statistical study of the vertical structure of traveling planetary-scale waves. *Mon. Wea. Rev.*, **96**, 12–22.

Derome, J., and A. Wiin-Nielsen, 1971: The response of a middle-latitude model atmosphere to forcing by topography and stationary heat sources. *Mon. Wea. Rev.*, **99**, 564–576.

Dickinson, R. E., 1968: Planetary Rossby waves propagating vertically through weak westerly wind wave guides. *J. Atmos. Sci.*, **25**, 984–1002.

Döös, B. R., 1962: The influence of exchange of sensible heat with the earth's surface on the planetary flow. *Tellus*, **14**, 133–147.

Eady, E. J., 1949: Long waves and cyclone waves. *Tellus*, **1**, 33–52.

Egger, J., 1976a: The linear response of a hemispheric two-level primitive equations model to forcing by topography. *Mon. Wea. Rev.*, **104**, 351–364.

——, 1976b: On the theory of the steady perturbations in the troposphere. *Tellus*, **28**, 381–390.

Eliasen, E. and B. Machenhauer, 1965: A study of fluctuation of the atmospheric planetary flow patterns represented by spherical harmonics. *Tellus*, **17**, 220–238.

——, and ——, 1969: On the observed large-scale atmospheric wave motions. *Tellus*, **21**, 149–166.

Eliassen, A., and E. Palm, 1960: On the transfer of energy in the stationary waves. *Geofys. Publ.*, **22**, 1–23.

Fjørtoft, R., 1951: Stability properties of large-scale atmospheric disturbances. *Compedium of Meteorology*, Amer. Meteor. Soc., 454–463.

Gall, R., 1976a: A comparison of linear baroclinic instability theory with the eddy statistics of a general circulation model. *J. Atmos. Sci.*, **33**, 349–373.

——, 1976b: Structural changes of growing baroclinic waves. *J. Atmos. Sci.*, **33**, 374–390.

——, 1976c: The effects of released latent heat in growing baroclinic waves. *J. Atmos. Sci.*, **33**, 1686–1701.

Gambo, K., 1950: The criteria for stability of the westerlies. *Geophys. Notes Japan*, **3**, 1–13.

——, 1956: The topographical effect upon the jet stream in the westerlies. *J. Meteor. Soc., Japan*, **34**, 24–28.

Garcia, R. V., and R. Norscini, 1970: A contribution to the baroclinic instability problem. *Tellus*, **22**, 239–250.

——, and J. E. Geisler, 1974: Vertical structure of stationary planetary waves in the presence of altitude-dependent zonal winds and dissipation. *J. Geophys. Res.*, **79**, 5613–5624.

Geisler, J. E., and R. E. Dickinson, 1975: External Rossby modes on a β-plane with vertical wind shear. *J. Atmos. Sci.*, **32**, 2082–2093.

Gent, P. R., 1974: Baroclinic instability of a slowly varying zonal flow. *J. Atmos. Sci.*, **31**, 1983–1994.

——, 1975: Baroclinic instability of a slowly varying zonal flow. Part 2, *J. Atmos. Sci.*, **31**, 2094–2102.

Green, J. S. A., 1960: A problem in baroclinic stability. *Quart. J. Roy. Meteor. Soc.*, **86**, 237–251.

Hartmann, D. L., 1974: Time spectral analysis of mid-latitude disturbances. *Mon. Wea. Rev.*, **102**, 348–362.

Hayashi, Y., 1971: A generalized method of resolving disturbances into progressive and retrogressive waves by space Fourier and time cross-spectral analyses. *J. Meteor. Soc. Japan*, **49**, 125–128.

——, 1974: Spectral analysis of tropical disturbances appearing in a GFDL general circulation model. *J. Atmos. Sci.*, **31**, 180–218.

——, 1977: On the coherence between progressive and retrogressive waves and a partition of space-time power spectra into standing, and traveling parts. (Submitted to *J. Appl. Meteor.*)

Hirota, I., 1968a: Planetary waves in the upper stratosphere in early 1966. *J. Meteor. Soc. Japan*, **46**, 418–430.

——, 1968b: On the dynamics of long and ultra-long waves in a baroclinic zonal current. *J. Meteor. Soc. Japan*, **46**, 234–249.

——, and Y. Sato, 1969: Periodic variation of the winter stratospheric circulation and intermittent vertical propagation of planetary waves. *J. Meteor. Soc. Japan*, **47**, 390–402.

——, 1971: Excitation of planetary Rossby waves in the winter stratosphere by periodic forcing. *J. Meteor. Soc. Japan*, **49**, 439–449.

Holloway, J. L., Jr., and S. Manabe, 1971: Simulation of climatology by a global general circulation model. *Mon. Wea. Rev.*, **99**, 335–370.

Holopainen, E. D., 1970: An observational study of the energy balance of the stationary disturbances in the atmosphere. *Quart. J. Roy. Meteor. Soc.*, **96**, 626–644.

Holton, J. R., 1973: On the trapping of unstable baroclinic waves. *J. Atmos. Sci.*, **31**, 2220–2222.

——, 1975: The dynamic meteorology of the stratosphere and mesosphere. *Meteor. Monogr.*, No. 37, 218 pp.

Iwashima, T., 1973: Observational studies of the ultra-long waves in the atmosphere (I) Part 1. Daily behavior of the quasi-stationary and traveling ultra-long waves during the stratospheric sudden warming. *J. Meteor. Soc. Japan*, **51**, 209–229.

——, 1974: Observational studies of the ultra-long waves in the atmosphere (II) Part 2. Ultra-long wave energy process during the stratospheric sudden warming. *J. Meteor. Soc. Japan*, **52**, 120–142.

Julian, P. R., 1971: Some aspects of variance spectra of synoptic-scale tropospheric wind components in mid-latitudes and in the tropics. *Mon. Wea. Rev.*, **99**, 954–965.

Kao, S. K., 1968: Governing equations and spectra for atmospheric motion and transports in frequency-wavenumber space. *J. Atmos. Sci.*, **25**, 32–38.

——, and L. L. Wendell, 1970: The kinetic energy of the large-scale atmospheric motion in wavenumber-frequency space: I. Northern Hemisphere. *J. Atmos. Sci.*, **27**, 359–375.

——, and J. Sagendorf, 1970: The large-scale meridional transport of sensible heat in wavenumber-frequency space. *Tellus*, **22**, 172–185.

——, C. Y. Tsay and L. L. Wendell, 1970: The meridional transport of angular momentum in wavenumber-frequency space. *J. Atmos. Sci.*, **27**, 614–626.

Kasahara, A., and W. M. Washington, 1971: General circulation experiments with a six-layer NCAR model, including orography, cloudiness, and surface temperature calculations. *J. Atmos. Sci.*, **28**, 657–701.

——, T. Sasamori and W. M. Washington, 1973: Simulated experiments with a 12-layer stratospheric global circulation model. I. Dynamical effect of the earth's orography and thermal influence of continentality. *J. Atmos. Sci.*, **30**, 1229–1251.

Kubota, S., and M. Iida, 1954: Statistical characteristics of the atmospheric disturbances. *Pap. Meteor. Geophys.*, **5**, 22–34.

Kuo, H. L., 1949: Dynamic instability of two dimensional non-divergent flow in a barotropic atmosphere. *J. Meteor.*, **6**, 105–122.

——, 1952: Three-dimensional disturbances in a baroclinic zonal current. *J. Meteor.*, **9**, 260–277.

——, 1953: The stability properties and structure of disturbances in a baroclinic atmosphere. *J. Meteor.*, **10**, 235–243.

——, 1973: Dynamics of quasi-geostrophic flows and instability theory. *Advances in Applied Mechanics*, Vol. 13, Academic Press, 248–330.

Kurihara, Y., and J. L. Holloway, Jr., 1967: Numerical integration of a nine-level global primitive equation model formulated by the box method. *Mon. Wea. Rev.*, **95**, 509–530.

Manabe, S., and T. B. Terpstra, 1974: The effects of mountains on the general circulation of the atmosphere as identified by numerical experiments. *J. Atmos. Sci.*, **31**, 3–42.

——, and J. D. Mahlman, 1976: Simulation of seasonal and inter-hemispheric variations in the stratospheric circulation. *J. Atmos. Sci.*, **33**, 2185–2217.

——, J. Smagorinsky and R. F. Strickler, 1965: Simulated climatology of a general circulation model with a hydrologic cycle. *Mon. Wea. Rev.*, **93**, 769–798.

——, D. G. Hahn and J. L. Holloway, Jr., 1974: The seasonal variation of the tropical circulation as simulated by a global model of the atmosphere. *J. Atmos. Sci.*, **31**, 43–83.

——, J. Smagorinsky, J. L. Holloway, Jr. and H. M. Stone, 1970: Simulated climatology of a general circulation model with a hydrologic cycle. III. Effects of increased horizontal computational resolution. *Mon. Wea. Rev.*, **98**, 175–212.

Matsuno, T., 1970: Vertical propagation of stationary planetary waves in the winter Northern Hemisphere. *J. Atmos. Sci.*, **27**, 871–883.

McIntyre, M. E., 1970: On the non-separable baroclinic parallel flow instability problem. *J. Fluid Mech.*, **40**, 273–306.

Mintz, Y., 1965: Very long-term global integration of the primitive equations of atmospheric motion. WMO Tech. Note No. 66, 141–167.

Muench, H. S., 1965: On the dynamics of the winter stratosphere circulation *J. Atmos. Sci.*, **22**, 349–360.

Murakami, T., 1967: Vertical transfer of energy due to stationary disturbances induced by topography and diabatic heat sources and sinks. *J. Meteor. Soc. Japan*, **45**, 205–231.

Newell, R. E., D. G. Vincent, T. G. Dopplick, D. Ferruzza and J. W. Kidson, 1970: The energy balance of the global atmosphere. *Global Circulation of the Atmosphere.* G. A. Corby, Ed., Roy. Meteor. Soc., 42–90.

Nitta, T., M. Nanbu and M. Yoshizaki, 1973: Wave disturbances over the China Continent and the Eastern China Sea in February, 1968. *J. Meteor. Soc. Japan*, **51**, 11–27.

Oort, A. H., 1964: On the energetics of the mean and eddy circulations in the lower stratosphere. *Tellus*, **16**, 309–327.

——, and E. M. Rasmusson, 1971: Atmospheric circulation statistics. NOAA Prof. Pap. 5.

Pedlosky, J., 1964a: The stability of currents in the atmosphere and ocean: Part I. *J. Atmos. Sci.*, **21**, 201–219.

——, 1964b: The stability of currents in the atmosphere and the ocean. Part II. *J. Atmos. Sci.*, **21**, 342–353.

Petterssen, S., 1956: *Weather Analysis and Forecasting*, Vol. 2. McGraw-Hill, 266 pp.

Phillips, N. A., 1957: A coordinate system having some special advantages for numerical forecasting. *J. Meteor.*, **14**, 184–185.

Pratt, R. W., and J. W. Wallace, 1976: Zonal propagation characteristics of large-scale fluctuations in the mid-latitude troposphere. *J. Atmos. Sci.*, **33**, 1184–1194.

Reed, R. J., J. L. Wolfe and H. Nishimoto, 1963: A spectral analysis of the energetics of the stratospheric warming of early 1957. *J. Atmos. Sci.*, **20**, 265–275.

Saltzman, B., 1968: Surface boundary effects on the general circulation and macroclimate: A review of the theory of the quasi-stationary perturbations in the atmosphere. *Meteor. Monogr.*, No. 30, 4–19.

——, 1970: Large-scale atmospheric energetics in the wavenumber domain. *Rev. Geophys.*, **8**, 289–302.

——, and F. E. Irsch III, 1972: Note on the theory of topographically forced planetary waves in the atmosphere. *Mon. Wea. Rev.*, **100**, 441–444.

Sankar-Rao, M., 1965: Continental elevation influence on the stationary harmonics of the atmosphere motion. *Pure Appl. Geophys.*, **60**, 145–159.

——, and B. Saltzman, 1969: On a steady state theory of global monsoons. *Tellus*, **21**, 308–330.

Sato, Y., 1974: Vertical structure of quasi-stationary planetary waves in several winters. *J. Meteor.*, **52**, 272–281.

——, 1976: Transient planetary waves in the winter stratosphere. Submitted to *J. Meteor. Soc.*

Simmons, A. J., 1974a: Planetary-scale disturbances in the polar winter stratosphere. *Quart. J. Roy. Meteor. Soc.*, **100**, 76–108.

——, 1974b: The meridional scale of baroclinic waves. *J. Atmos. Sci.*, **31**, 1515–1525.

——, 1975: Reply (to P. H. Stone). *J. Atmos. Sci.*, **32**, 990–991.

——, and B. J. Hoskins, 1976: Baroclinic instability on the sphere: Normal modes of primative and quasi-geostrophic equations. *J. Atmos. Sci.*, **33**, 1454–1477.

Simons, T. J., 1972: The nonlinear dynamics of cyclone waves. *J. Atmos. Sci.*, **29**, 38–52.

Smagorinsky, J., 1953: The dynamical influence of large-scale heat sources and sinks on the quasi-stationary mean motions of the atmosphere. *Quart. J. Roy. Meteor. Soc.*, **79**, 343–366.

Song, R. T., 1971a: A numerical study of the three dimensional structure and energetics of unstable disturbances in zonal currents. Part I. *J. Atmos. Sci.*, **28**, 549–564.

——, 1971b: A numerical study of the three-dimensional structure and energetics of unstable disturbances in zonal currents. Part II. *J. Atmos. Sci.*, **28**, 565–586.

Stone, P. H., 1969: The meridional structure of baroclinic waves. *J. Atmos. Sci.*, **26**, 376–389.

——, 1975: Comments on "The meridional scale of baroclinic waves". *J. Atmos. Sci.*, **32**, 988–990.

van Loon, H., R. L. Jenne and K. Labitzke, 1973: Zonal harmonic standing waves. *J. Geophys. Res.*, **78**, 4463–4471.

Van Mieghem, J., 1961: Zonal harmonic analysis of the northern hemisphere geostrophic wind field. IUGG Monogr. No. 8, 57 pp.

Wiin-Nielsen, A., 1971a: On the motion of various vertical modes of transient very long waves. Part. I. Beta approximation. *Tellus*, **23**, 87–98.

——, 1971b: On the motion of various vertical modes of transient very long waves. Part II. The spherical case. *Tellus*, **23**, 207–217.

Williams, G. P., 1974: Generalized Eady waves. *J. Fluid Mech.*, **62**, 643–655.

——, and J. B. Robinson, 1974: Generalized Eady waves with Ekman pumping. *J. Atmos. Sci.*, **31**, 1768–1776.

Williams, J., 1976: Zonal harmonic standing waves in the NCAR global circulation model. *Mon. Wea. Rev.*, **104**, 249–259.

Willson, M. A. G., 1975: A wavenumber-frequency analysis of large-scale tropospheric motions in the extratropical northern hemisphere. *J. Atmos. Sci.*, **32**, 478–488.